


Dear Author,

Please, note that changes made to the HTML content will be added to the article before publication, but are not reflected in this PDF.

Note also that this file should not be used for submitting corrections.

AUTHOR QUERY FORM

 ELSEVIER	Journal: YCRES	Please e-mail or fax your responses and any corrections to:
	Article Number: 3095	E-mail: corrections.esch@elsevier.tnq.co.in Fax: +91 44 24426088

Dear Author,

Please check your proof carefully and mark all corrections at the appropriate place in the proof (e.g., by using on-screen annotation in the PDF file) or compile them in a separate list. Note: if you opt to annotate the file with software other than Adobe Reader then please also highlight the appropriate place in the PDF file. To ensure fast publication of your paper please return your corrections within 48 hours.

For correction or revision of any artwork, please consult <http://www.elsevier.com/artworkinstructions>.

Any queries or remarks that have arisen during the processing of your manuscript are listed below and highlighted by flags in the proof.

Location in article	Query / Remark: Click on the Q link to find the query's location in text Please insert your reply or correction at the corresponding line in the proof
Q1	The citation 'Jenkyns, 1995; McArthur and Howart, 2004; Ruberti et al., 2006; Follmi and Godet (2013); Ruberti et al., 2006a; Schlagintweit and Sanders (2008); Frijia and Parente et al., 2008; Frijia and Parente, 2008' have been changed to match the author name/date in the reference list. Please check.
Q2	Please update Ref. 'Arriaga et al., 2014'.
Q3	Please expand the journal title in Ref. 'Cherchi and Schroeder, 1990'.
Q4	Please confirm that given names and surnames have been identified correctly.
	<div style="border: 1px solid black; padding: 5px;"> <p>Please check this box or indicate your approval if you have no corrections to make to the PDF file</p> <div style="display: inline-block; border: 1px solid black; width: 40px; height: 40px; vertical-align: middle;"></div> </div>

Thank you for your assistance.

Contents lists available at [ScienceDirect](#)

Cretaceous Research

journal homepage: www.elsevier.com/locate/CretRes

Highlights

- We present a detailed C- and Sr-isotope stratigraphy of S-Italy Carbonate Platform.
- Chronostratigraphic calibration of foraminiferal biozones by isotope stratigraphy.
- Four new sub-zones are proposed.
- Range of some key species is synchronous across different Tethyan platforms.

UNCORRECTED PROOF



Contents lists available at ScienceDirect

Cretaceous Research

journal homepage: www.elsevier.com/locate/CretRes

Carbon and strontium isotope stratigraphy of the Upper Cretaceous (Cenomanian–Campanian) shallow-water carbonates of southern Italy: Chronostratigraphic calibration of larger foraminifera biostratigraphy

Gianluca Frijia^{a,*}, Mariano Parente^b, Matteo Di Lucia^c, Maria Mutti^a

^a Institut für Erd- und Umweltwissenschaften, Universität Potsdam, House 27, Karl-Liebknecht-Str. 24–25, 14476 Potsdam-Golm, Germany

^b Dipartimento di Scienze della Terra, dell'Ambiente e delle Risorse, Università degli Studi di Napoli Federico II, Largo San Marcellino 10, 80138 Napoli, Italy

^c RPS Energy, Goldvale House, 27–41 Church Street West, Woking, Surrey GU21 6DH, United Kingdom

ARTICLE INFO

Article history:

Received 13 September 2014

Accepted in revised form 4 November 2014

Available online xxx

Keywords:

Strontium isotope stratigraphy

Carbon isotope stratigraphy

Biostratigraphy

Larger foraminifera

Upper Cretaceous

Apennine Carbonate Platform

Southern Italy

ABSTRACT

Shallow-water carbonates are invaluable archives of past global change. They hold the record of how neritic biologic communities reacted to palaeoenvironmental changes. However, attempts to decipher these geological archives are often severely hampered by the low stratigraphic resolution attained by biostratigraphy. This is particularly the case for the Upper Cretaceous carbonate platforms of the central Tethyan realm: their biostratigraphy suffers from very low resolution and poor correlation with the standard biochronologic scales based on ammonites, planktic foraminifers and calcareous nannoplankton.

In this paper we show how this problem can be tackled by integrating biostratigraphy with isotope stratigraphy. We present a detailed record of the benthic foraminiferal biostratigraphy and carbon and strontium isotope stratigraphy of three upper Cenomanian–middle Campanian sections belonging to the Apennine Carbonate Platform of southern Italy. For the upper Cenomanian–Turonian interval, the carbon isotope curves of the studied sections are easily correlated to the reference curve of the English Chalk. The correlation is facilitated by the matching of the prominent positive excursion corresponding to the Oceanic Anoxic Event 2. For the Coniacian–middle Campanian interval, the correlation is mainly based on strontium isotope stratigraphy. We use the $^{87}\text{Sr}/^{86}\text{Sr}$ ratios of the low-Mg calcite of well preserved rudist shells to obtain accurate chronostratigraphic ages for many levels of the three studied sections. The ages obtained by Sr isotope stratigraphy are then used to better constrain the matching of the carbon isotope curves.

From the high-resolution chronostratigraphic age-model established by isotope stratigraphy, we derive the chronostratigraphic calibration of benthic foraminiferal biostratigraphic events. For the first time the benthic foraminiferal biozones of the Apennine Carbonate Platform can be accurately correlated to the standard ammonite biozonation. This result is of great relevance because the biostratigraphic schemes of other carbonate platforms in the central and southern Tethyan realm are largely based on the same biostratigraphic events.

© 2014 Published by Elsevier Ltd.

1. Introduction

Carbonate platforms were widespread in the Tethyan region during the Cretaceous (Kiessling et al., 2003; Philip, 2003; Skelton, 2003). These complex sedimentary systems responded to changing environmental conditions with changes in the relative abundance of the main carbonate producers and with repeated phases of inception, growth, retreat and demise. Therefore, they potentially

* Corresponding author. Institut für Erd- und Umweltwissenschaften, House 27, Karl-Liebknecht-Str. 24–25, 14476 Potsdam-Golm, Germany. Tel.: +49 3319775848.

E-mail addresses: frijia@geo.uni-potsdam.de (G. Frijia), maparent@unina.it (M. Parente), diluciam@rpsgroup.com (M. Di Lucia), Maria.Mutti@geo.uni-potsdam.de (M. Mutti).

preserve a detailed record of how neritic biologic communities reacted to changes in climatic and oceanographic conditions and sea-level changes. However, the study of this invaluable palaeoenvironmental and palaeobiological archive is often severely hampered by the low stratigraphic resolution of biostratigraphy of Cretaceous carbonate platforms and by the lack of precise correlation with coeval hemipelagic and pelagic successions. Most of what we know on the Cretaceous climate and oceans has been derived from the study of deep-water successions, which are generally accurately dated by means of chronostratigraphically significant macro- and microfossils (ammonites, calcareous plankton and nannoplankton), sometimes supplemented by other high-resolution stratigraphic tools, like chemo-, magneto- and cyclostratigraphy. On the contrary, biozonations of Cretaceous carbonate platforms, mainly based on calcareous algae and larger foraminifers, usually have a much coarser resolution and, generally, a poorly constrained chronostratigraphic calibration. Some notable exceptions include the biostratigraphic scheme of orbitolinid foraminifers in the Lower Cretaceous French-Swiss Urgonian Platform and Arabian Platform, for which chronostratigraphic calibrations, albeit controversial, have been proposed (Arnaud et al., 1998; Arnaud, 2005; Clavel et al., 2009, 2010; Schroeder et al., 2010), and the biozonation of orbitoidal foraminifers for Campanian-Maastrichtian peri-Mediterranean carbonate platforms, which is reasonably well calibrated to calcareous plankton (van Gorsel et al.,

1978; Caus et al., 1996), but only applicable to open platform settings. Finally, Steuber and Schlüter (2012) proposed recently a chronostratigraphical calibration of rudist bivalve biozones using Sr-isotopes stratigraphy.

The problem of low resolution is particularly acute for the Upper Cretaceous carbonate platforms of the central and southern Tethyan area, as shown by the most widely used biostratigraphic schemes (De Castro, 1991, southern Apennines; Chiocchini et al., 2008, central Apennines; Fleury, 1980, Greece; Velic, 2007, Adriatic platform; see Fig. 1). With a few exceptions, each biozone covers a time-interval >4 Myr. The most recent biozonation of the Adriatic platform (Velic, 2007) presents a slightly higher resolution, at least in the Cenomanian-Santonian interval (average resolution is about 2 Myr per biozone, see Fig. 1). However, this biozonation makes use of virtually any available biostratigraphic event and it is highly improbable that all these events can be used outside of the Adriatic platform. Even more critical than their low resolution, is the problem posed by the chronostratigraphic calibration of these biozonal schemes. Ammonites, calcareous plankton and nannoplankton are virtually absent in these carbonate platforms and direct correlation to deep-water successions has not been established. As a result, the chronostratigraphic age of the biozones is poorly constrained. This is explicitly acknowledged in De Castro (1991) and Chiocchini et al. (2008). No evidence is cited in Velic (2007, p. 2) for the calibration of the Turonian-Maastrichtian

Stages	duration (My)	BIOZONES Fleury, 1980 (Gavrovo-Tripolitza carbonate platform)	BIOZONES De Castro, 1991 (Apennine Carbonate Platform, Campania)	BIOZONES Velic, 2007 (Adriatic Platform, karst Dinarides)	BIOZONES Chiocchini et al., 2008 (Apennine Carbonate Platform, Lazio-Abruzzo)	
Maastrichtian	5.1	CsB7 <i>R. liburnica</i>		<i>Fleuryana adriatica</i>	<i>Discorbidae & Miliolidae</i>	
Campanian	12.9	CsB6 <i>Rhapydioninae</i>	<i>Accordiella conica</i> & <i>Moncharmontia apenninica</i>	<i>M. cuvillieri & R. liburnica</i>	<i>Orbitoides media</i>	
		CsB5 <i>Orbitolinides K</i> and <i>M. apenninica</i>		<i>C. lecalvezae & M. cuvillieri</i>		
		CsB4 <i>M. lata</i>		<i>Calveziconus lecalvezae</i>		
Santonian	2.3	CsB3 <i>P. sphaeroidea</i>		<i>K. tergestina</i>	<i>Accordiella conica</i> & <i>Rotorbinella scarsellai</i>	
Coniacian	3.5		<i>M. lata</i>			
Turonian	4.2		<i>"Pseudocyclammina" spp.</i>	<i>D. schlumbergeri & M. lata</i>	<i>Nezzazatinella cf. aegyptiaca</i> & <i>Nummoloculina cf. irregularis</i>	
				<i>S. samnitica & D. schlumbergeri</i>		
Cenomanian	6.1	CsB2 <i>B. balcanica</i>	<i>C. fraasi & C. gradata</i>	<i>P. sphaeroidea & S. samnitica</i>	<i>C. gradata & P. reicheli</i>	
		CsB1 <i>S. gr. vialli</i>		<i>C. gradata & P. sphaeroidea</i>		
				<i>C. gradata</i>		<i>P. dubia & P. laurinensis</i>
				<i>V. radoicicae & C. gradata</i>		<i>Ostracoda & Miliolidae</i>
	<i>P. balcanica & C. conica</i>					
		<i>Chrysalidina gradata</i>				
			<i>C. conica & C. cuvillieri</i>			

Fig. 1. Late Cenomanian-Maastrichtian biostratigraphy of central Tethyan carbonate platforms. All these schemes suffer of low resolution and poorly constrained chronostratigraphic calibration. Substage duration is after Gradstein et al. (2004).

carbonate platform biozones. An overly optimistic impression of a perfect chronostratigraphic calibration is also conveyed by some compilations of the ranges of selected taxa of larger foraminifers (Hardenbol et al., 1998; Ogg and Ogg, 2008), which unfortunately lack any reference to supporting data.

In the last decades, isotope stratigraphy has emerged as a powerful stratigraphic tool that, when used in combination with classical biostratigraphy, has the potential of highly improving time-resolution and of solving the problem of global correlation across different facies and different palaeobioprovinces. The most successful isotopic methods rely on the secular fluctuations of carbon and strontium isotope ratios recorded by marine carbonates (see Weissert et al., 2008; McArthur et al., 2012, for recent reviews).

Perturbations of the global carbon cycle, involving changes in the fluxes and amounts of carbon stored into the different reservoirs, are mirrored by excursions in the carbon-isotope record of marine carbonates and organic matter. These oscillations have been increasingly utilised for dating and correlation of Cretaceous pelagic and hemipelagic successions since the pioneering work of Scholle and Arthur (1980) showed the occurrence of some prominent carbon isotope excursions that could be correlated from section to section at a global scale. The state-of-the-art reference curve for the Late Cretaceous (Cenomanian–Campanian) has been obtained by piecing together the isotopic record of seven Chalk successions in England (Jarvis et al., 2006). The curve is perfectly calibrated to the geological time-scale through macrofossil events, marker-bed lithostratigraphy and six bentonite horizons. It contains some major positive $\delta^{13}\text{C}$ excursions of up to +2‰, plus many minor events of smaller amplitude, which can be successfully correlated from the Boreal to the Tethyan realm (see Wendler, 2013, for a recent review). Application of carbon isotope stratigraphy to shallow-water carbonates is more problematic because the global oceanic signal can be overprinted and masked to a great extent by local palaeoceanographic conditions, complex biological fractionation effects, changes of dominant mineralogy (aragonite vs calcite) and diagenetic processes (see Mutti et al., 2006; Immenhauser et al., 2008; Föllmi and Godet, 2013; Wendler, 2013; and references therein). Moreover, changes of accumulation rate, undisclosed stratigraphic gaps and the lack of reliable chronostratigraphic tie-points can severely hamper correlation between the curves recovered from shallow-water carbonate sections and the pelagic reference curves (see Di Lucia et al., 2012, for a discussion of some common pitfalls). Despite these limitations, carbon isotope stratigraphy has been increasingly applied to Cretaceous platform carbonates during the last 20 years (Wagner, 1990; Jenkyins, 1995; Vahrenkamp, 1996; Ferreri et al., 1997; Grötsch et al., 1998; Davey and Jenkyins, 1999; Wissler et al., 2003, 2004; D'Argenio et al., 2004; Immenhauser et al., 2005; Parente et al., 2007, 2008; Amodio et al., 2008; Burla et al., 2008; Elrick et al., 2008; Millán et al., 2009, 2011; Huck et al., 2010, 2011; Strohmenger et al., 2010; Vahrenkamp, 2010; Najjarro et al., 2011; Tesovic et al., 2011; Di Lucia et al., 2012; Husinec et al., 2012; Korbar et al., 2012; Stein et al., 2012; Huck et al., 2013; Papp et al., 2013).

Strontium isotope stratigraphy (SIS) is a well established chemostratigraphic method (McArthur, 1994; McArthur and Howarth, 2004; McArthur et al., 2012). It is based on the empirical observation that the Sr isotope ratio of the ocean, recorded by marine carbonates and phosphates, has varied during the past and on the assumption (verified for the present ocean; DePaolo and Ingram, 1985) that at any moment the Sr isotope ratio of the ocean is homogeneous, because the residence time of Sr is much longer than the ocean mixing time. By assembling a database of the Sr isotope ratios of well preserved and well dated marine precipitates, a marine reference curve for the past 590 Ma of geologic history has

been built and continuously refined during the last decades (McArthur et al., 2001; McArthur and Howarth, 2004; McArthur et al., 2012). The use of the reference curve as a stratigraphic tool is facilitated by its conversion into a look-up table, giving the numerical ages and the 95% confidence limits for any value of $^{87}\text{Sr}/^{86}\text{Sr}$ interpolated in steps of 0.000001. The method has proven especially useful in dating and correlation of Upper Cretaceous shallow-water carbonates, which often lack chronostratigraphically significant markers like ammonites, planktic foraminifers and calcareous nannoplankton (Steuber, 2001, 2003; Steuber et al., 2002, 2005, 2007; Masse and Steuber, 2007; Frijia and Parente, 2008a,b; Schlüter et al., 2008; Boix et al., 2011; Huck et al., 2011; Vicedo et al., 2011; Steuber and Schlüter, 2012; Caus et al., 2013; Vicedo et al., 2013; Albrich et al., 2014).

In this paper we integrate SIS and carbon isotope stratigraphy for building a high-resolution age-model for the Upper Cretaceous shallow-water limestones of the Apennine Carbonate Platform of southern Italy. Carbon-isotope stratigraphy outperforms SIS in the upper Cenomanian–lower Turonian interval, where accurate correlation with the reference curve of the English Chalk is favoured by the prominent positive excursion associated with the CTB event (Bonarelli event, OAE2; Parente et al., 2007; Frijia and Parente, 2008a,b). For the middle Turonian to Campanian, SIS is used to establish a first version of the age model and to help the correlation of the $\delta^{13}\text{C}$ curves of the ACP with the reference curve. Integration of the two methods allows further refinement and validation of the age-model.

From our chemostratigraphically constrained age-model we derive the first accurate chronostratigraphic calibration of the ranges of some species of benthic foraminifers that are widely used in the biostratigraphy of central and southern Tethyan Late Cretaceous carbonate platforms.

2. The Apennine Carbonate Platform: palaeogeography, stratigraphy and facies models

The Apennine Carbonate Platform (ACP) of southern Italy comprises Mesozoic carbonate successions deposited in shallow tropical waters at the south-western margin of the Neo-Tethys Ocean. They were part of a palaeotectonic domain, variously called Adria or Apulia, which has been alternatively interpreted as a promontory of the African continent (Channell et al., 1979; Schettino and Turco, 2011) or as an independent continental block, separated from Africa by an oceanic corridor (Dercourt et al., 1986; Stampfli and Mosar, 1999; see also Bosellini, 2002, for a review on the promontory versus microplate controversy). In the reconstructions of the Mesozoic palaeogeography of Adria, the ACP is an element of a more or less articulated system of carbonate platforms separated by deep basins (D'Argenio et al., 1973; Mostardini and Merlini, 1986; Sgroso, 1988; Menardi Noguera and Rea, 2000; Patacca and Scandone, 2007). Shallow-water carbonate sedimentation started in the Middle Triassic and was established over large areas in the Late Triassic, persisting with minor interruptions until the Late Cretaceous. After a long phase of subaerial exposure, neritic carbonate sedimentation was locally re-established in the late Paleocene–Eocene with the foraminiferal limestones and characean marls of the Trentinara Formation (Selli, 1962) and again in the early Miocene, with the red algae and bryozoan limestones of the Roccadaspide, Cerchiara and Cusano Formation (Selli, 1957). This last phase of shallow-water carbonate sedimentation was eventually terminated in the middle Miocene by drowning below the photic zone, followed by deposition of deep-water siliciclastics (Sgroso, 1998; Lirer et al., 2005; Patacca and Scandone, 2007).

The total thickness of the exposed portion of the Mesozoic ACP is about 4000 m (D'Argenio and Alvarez, 1980; Frijia et al., 2005).

The maximum thickness of the Cretaceous carbonates is about 1000–1200 m. In particular, the most complete successions show a thickness of 400–450 m between the upper Cenomanian, marked by the *Cisalveolina fraasi* (Gümbel) beds, and the base of the Trentinara Fm. (Sartoni and Crescenti, 1962). Following the abrupt disappearance of the high-diversity larger foraminiferal assemblages of the upper Cenomanian, which has been associated with the Oceanic Anoxic Event 2 (Parente et al., 2007, 2008), there is a 60–80 m thick poorly fossiliferous interval which is generally dated as Turonian. This is overlain by rudist-rich limestones that have been generally referred to as “Senonian” in age (e.g. Carannante et al., 1999). The depositional system and fossil associations of the “Senonian” rudist limestones have been described in several papers (e.g. Carannante et al., 1997, 1998, 1999, 2000; Ruberti et al., 2006, 2007). In a recent synthesis, two end-member depositional settings have been recognized on the basis of sedimentological, taphonomic and palaeontological characters (Simone et al., 2003). In the more external and/or high-energy areas, rudist lithosomes are thicker, grade laterally into clean bioclastic grainstone and are made of highly diversified rudist assemblages dominated by large hippuritids and thick shelled radiolitids and plagiopychids. In more internal and/or low-energy areas rudist-rich beds alternate with fine-grained foraminiferal limestones and are characterised by oligotypic rudist assemblages dominated by small radiolitids.

The lithostratigraphy of the Upper Cretaceous carbonates of the ACP has been recently redefined in the framework of the new edition of the geological map of Italy at 1:50,000 scale, coordinated by the Italian Geological Survey (project CARG). The successions studied in this work can be referred to the upper part of the “Calcare ad alveoline e dolomie laminare” Member (Alveolinid limestones and laminated dolomites Mb) and the overlying “Calcare a

radiolitidi” Formation (Radiolitid Limestones Fm) (Di Stefano et al., 2011; Servizio Geologico d’Italia, 2010).

3. Material and methods

3.1. Field work, sedimentology and biostratigraphy

In this study we investigated three sections of Upper Cretaceous shallow-water carbonates of the ACP, along an NW–SE transect from the Cilento promontory to the Campania-Lucania border (Fig. 2). The Mt. Coccovello section (40°02’50” N–15°42’24” E; fig. 2) was logged from a few metres below the first occurrence (FO) of *Cisalveolina fraasi* to the top of the Radiolitid Limestones Fm., marked by the base of the overlying Palaeocene–Eocene Trentinara Fm. The Mt. Varchera section (40°12’45” N–15°37’18” E, fig. 2) also starts a few metres below the FO of *C. fraasi*, goes through about 180 m of the Radiolitid Limestones but does not reach the base of the Trentinara Fm because of tectonic disturbance. The Trentinara section (40°23’39” N–15°07’37” E; fig. 2) is entirely within the Radiolitid Limestones Fm. and is capped by the Trentinara Fm. The upper Cenomanian–Turonian part of the Mt. Coccovello and Mt. Varchera sections were previously investigated by Parente et al. (2007, 2008) and Frijia and Parente (2008a,b). The rudists and facies of the Trentinara section have been previously discussed in several papers (Ruberti and Toscano, 2002; Cestari and Pons, 2004; Ruberti et al., 2006, 2007). The lithology, sedimentology and fossil content of the studied sections were described in the field at a dm-scale. Field observations were integrated with the study of about 750 thin sections. The biostratigraphic scheme presented in this paper incorporates some species that have been introduced in open nomenclature in previously published biozonations (e.g.

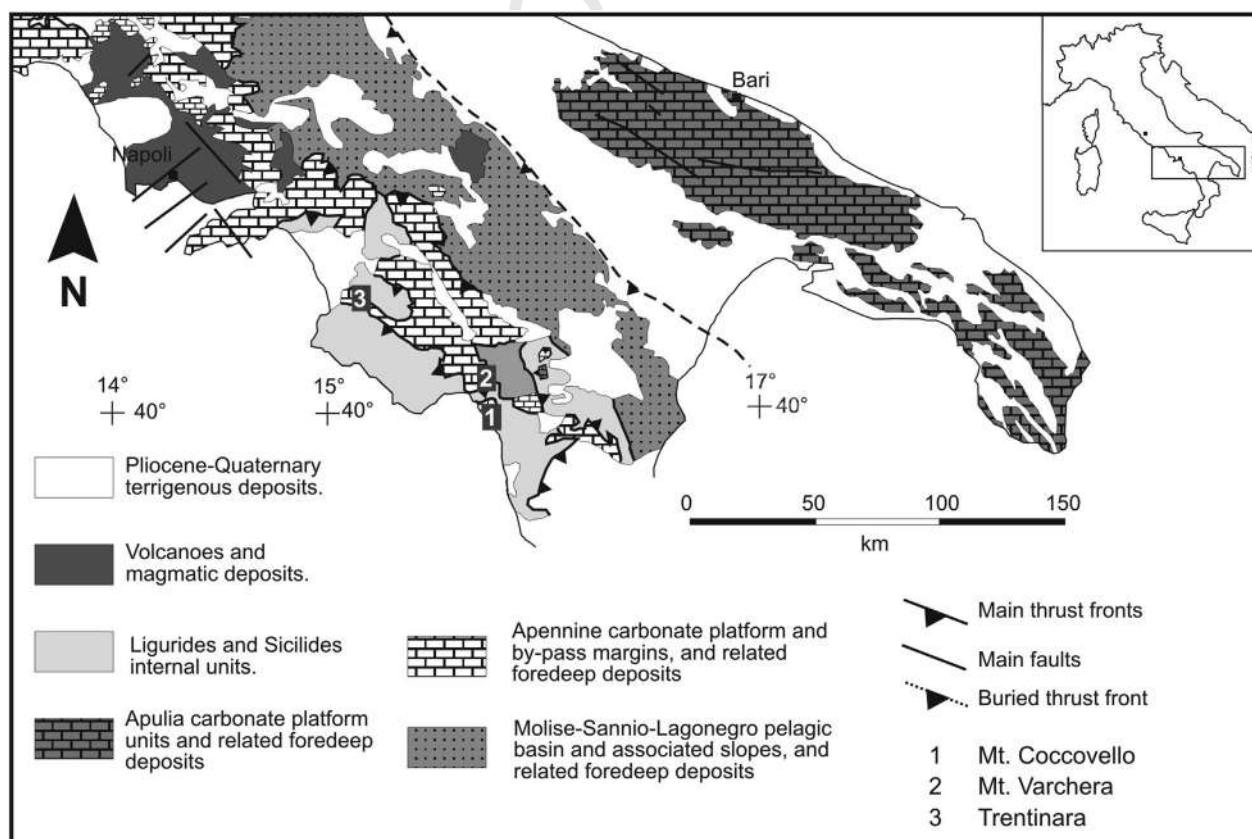


Fig. 2. Schematic geological map of the southern Apennines (modified from Bonardi et al., 1988), with location of the studied sections.

Nummoloculina cf. irregularis Decrouez and Radoičić and *Nezzazatinella cf. aegyptiaca* Said and Kenawy, see [Chiocchini et al., 1994, 2008](#)). A systematic revision of some of these taxa is beyond the scope of this work and is the object of a companion paper ([Arriaga et al., submitted for publication](#)). All the samples and thin sections used for the present paper are stored at the University of Naples Federico II (collection M. Parente) and at the University of Potsdam (collection G. Frijia).

3.2. Isotope geochemistry and concentrations of trace and major elements

Samples for carbon-isotope stratigraphy were collected at intervals ranging from 50 cm to 1.5 m, except where poor outcrop conditions dictated a larger spacing. Powders were produced by micro-drilling polished rock slabs with a tungsten carbide drill bit of 0.5 mm \varnothing . In most cases it was possible to obtain pure micrite by carefully selecting for microdrilling mudstones, wackestones or the micritic matrix of mud-dominated packstones and floatstones. Only for levels entirely made of grainy bioclastic facies, the analysed powder was obtained from the bulk rock. In any case, care was taken to avoid cement-filled cavities, veins and areas showing petrographic evidence of diagenetic alteration.

The oxygen and carbon isotope composition was analysed on a total of 745 samples, using a Finnigan Gas Bench II at the Institute for Geology, Mineralogy and Geophysics of the Ruhr-University of Bochum (refer to [Parente et al., 2007](#), for details on the analytical procedure). The results are reported as δ values with reference to the Vienna-Pee Dee Belemnite (VPDB). Precision (1σ), monitored by repeated analyses of international standards and of a laboratory standard, was $\pm 0.09\text{‰}$ for carbon and $\pm 0.13\text{‰}$ for oxygen isotopes. Replicate measurements gave reproducibility in the range of $\pm 0.1\text{‰}$ for $\delta^{13}\text{C}$ and $\pm 0.2\text{‰}$ for $\delta^{18}\text{O}$.

Eighty-one fragments of radiolite shells and three shells of undetermined bivalves were analysed for SIS. Whenever possible, multiple samples were collected from each stratigraphic level, in order to test the internal consistency of the data. The samples were selected in the field by a preliminary assessment of their preservation with a low magnification hand lens. Only compact-shelled radiolite specimens were chosen. Laboratory preparation and further screening of the selected shell fragments followed the method described in [Frijia and Parente \(2008b\)](#). In order to assess the preservation of the original shell microstructure, the samples were passed through a complete petrographic screening (optical microscope, cathodoluminescence, SEM). A further screening step was performed by analysing the elemental (Mg, Sr, Mn and Fe) composition of the shells. The micritic matrix and calcitic cements of some samples were also analysed in order to gain deeper insight into the diagenetic evolution. Concentration of Mg, Sr, Fe and Mn was determined with ICP-AES at the Geographisches Institut of the Ruhr-Universität of Bochum (refer to [Frijia and Parente, 2008b](#); [Boix et al., 2011](#) for analytical procedures and reproducibility of replicate analyses). Strontium isotope analyses were performed at the Institute for Geology, Mineralogy and Geophysics of the Ruhr-University (Bochum, Germany). After strontium separation by standard ion-exchange methods, strontium-isotope ratios were analysed on a Finnigan MAT 262 thermal-ionisation mass spectrometer and normalized to an $^{86}\text{Sr}/^{88}\text{Sr}$ value of 0.1194. The long term mean of modern seawater (USGS EN-1), measured at the Bochum isotope laboratory during the period when the samples were analysed, was 0.709158 ± 0.000004 (2 s.e., $n = 180$). The mean value of the USGS EN-1 standards run together with the samples analysed for this study is 0.709159 ± 0.000005 (2 s.e., $n = 22$). The $^{87}\text{Sr}/^{86}\text{Sr}$ ratios of the samples were adjusted to a value of 0.709175 for the USGS EN-1 standard, to be consistent with the

normalisation used in the compilation of the “look-up” table of [McArthur et al. \(2001\)](#); version 4: 08/04). A mean value was calculated when more than one sample was available for one stratigraphic level. When more than one level was sampled in a thin interval (less than 15 m), with no evidence of intervening stratigraphic gaps, we derived the numerical age from the mean value of all the samples. This procedure is based: a) on the assumption that significant changes of Sr isotope ratios are not expected to occur over time intervals much shorter than the Sr residence time (2 Ma), b) on an estimated long-term accumulation rate of a few tens of m/Myr. Following the assumption that the sedimentary dynamics of Upper Cretaceous rudist-bearing carbonates of the southern Apennines was similar to that of temperate carbonates ([Simone et al., 2003](#) and references therein), we use the accumulation rate for “cool-water” carbonates from [Schlager \(2000\)](#). The precision of the $^{87}\text{Sr}/^{86}\text{Sr}$ mean value for each stratigraphic level is given as 2 s.e. of the mean when the number of samples (n) is ≥ 4 . When $n < 4$, the precision is considered to be not better than the average precision of single measurements (2 s.e. = ± 0.000007) and is calculated from the standard deviation of the mean value of the standards run with the samples (± 0.000024 for $n = 1$, ± 0.000017 for $n = 2$ and ± 0.000014 for $n = 3$). The numerical ages of the samples analysed in this study were derived from the look-up table of [McArthur et al. \(2001\)](#), version 4: 08/04), which is tied to the Geological Time Scale of [Gradstein et al. \(2004\)](#); hereinafter GTS2004). Minimum and maximum ages were obtained by combining the statistical uncertainty (2 s. e.) of the mean values of the Sr-isotope ratios of the samples with the uncertainty of the seawater curve. The numerical ages were then translated into chronostratigraphic ages and corresponding standard biozones (ammonites, planktic foraminifera and calcareous nannoplankton) by reference to the GTS2004.

4. Results

4.1. Stratigraphy and facies

The studied sections show a very similar stratigraphy and facies evolution. They can all be ascribed to an inner platform setting. The Trentinara succession shows slightly more open marine facies whereas the most restricted ones occur at Mt. Coccovello, where peritidal cycles dominate the successions and subaerial exposure surfaces are more frequent. Five main lithofacies associations have been identified on the basis of texture, components (mainly skeletons) and sedimentary structures ([Fig. 3](#)):

LF1: characean-ostracod mudstone. This lithofacies generally makes medium beds (10–20 cm) at the top of LF2 (see below). It is dominated by mudstone textures but wackestones sporadically occur. The main skeletal components are characean oogons and ostracod shells, often with articulated valves. Subordinate (common to rare) *Decastronema kotori* Golubic, Radoičić and Seong-joo cyanobacteria are also present, together with rare *Thaumatoporella* algae and discorbids. Small vugs and bird-eyes occur frequently in this lithofacies as well as microbrecciated levels and circumgranular cracks. The sedimentological characters suggest a deposition in ephemeral supratidal ponds or in a brackish coastal lagoon.

LF2: *Thaumatoporella* mudstone to bindstone. This lithofacies occurs usually in medium to thick beds (10–40 cm) capping (or alternating with) LF4 or LF5 and showing different textures from mudstones to packstone/bindstone. According to the texture, components, sedimentary and diagenetic features, it can be further subdivided in:

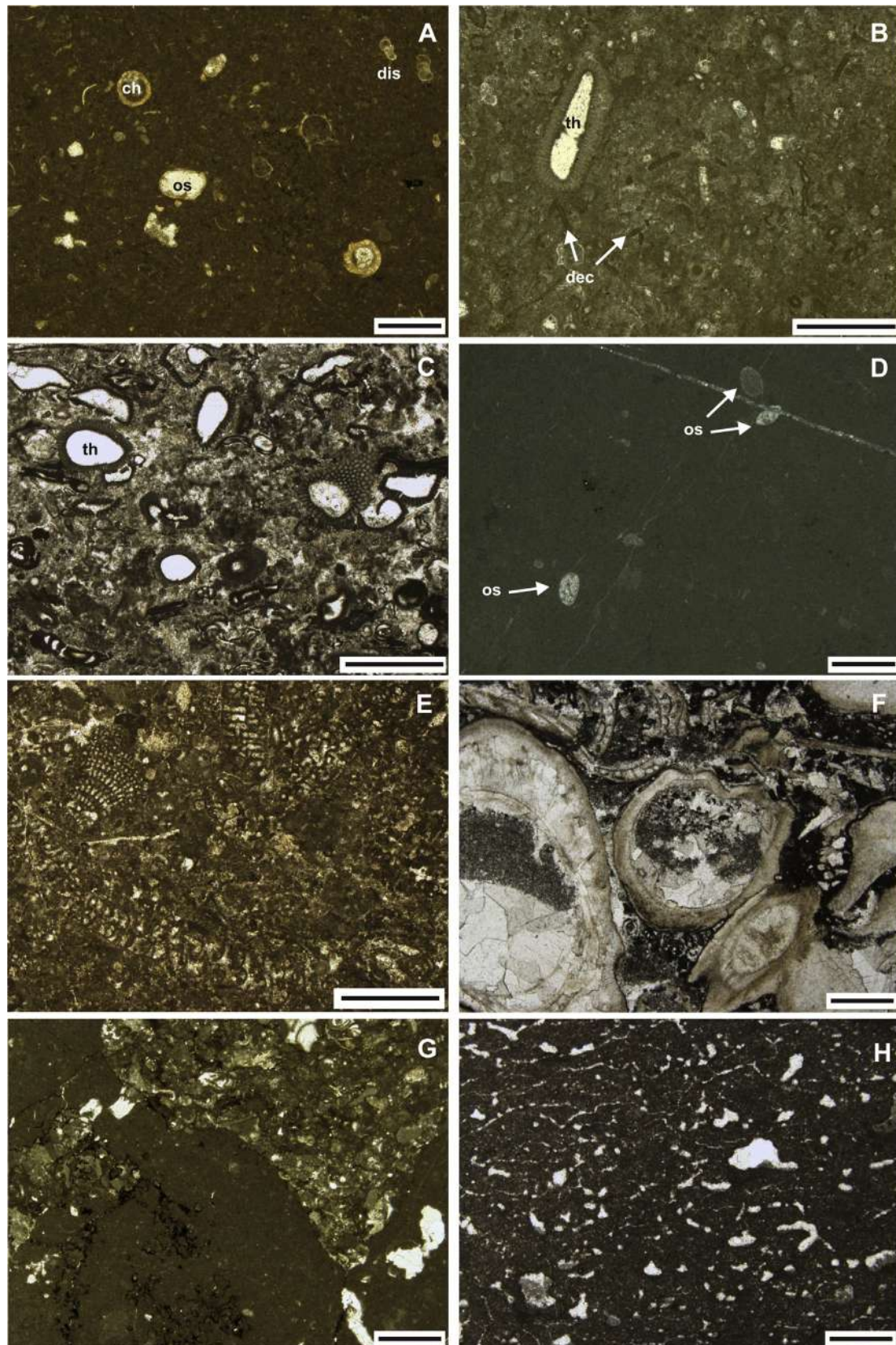


Fig. 3. Some representative microfacies of the studied sections. **A** characean-ostracod mudstone (LF1), ch: characean oogons, os: ostracods, dis: discorbids (P 428, Mt. Coccovello); **B** Thaumatoporella/Decastronema wackestone (LF2a), th: Thaumatoporella alga, dec: *Decastronema kotori* (P 929, Trentinara); **C** Thaumatoporella-foraminiferal wackestone (LF2b), th: Thaumatoporella alga (P 924, Trentinara); **D** ostracod-miliolid mudstone (LF3), os: ostracods (P 897, Trentinara); **E** Foraminiferal wackestone/packstone (LF4) (P 797, Trentinara); **F** Rudist rudstone (LF5) (P 962, Trentinara); **G** characean-ostracod mudstone (LF1) with dissolution cavities filled by Thaumatoporella-foraminiferal packstone (LF2) (P 552, Mt. Coccovello); **H** fenestral mudstone (LF3). The larger vugs have a geopetal fill of crystal silt followed by sparry calcite (P 916, Trentinara). Scale bar is 1 mm for all the photographs.

LF2a: *Thaumatoporella*/*Decastronema* mudstone-wackestone. This facies is dominated by *Thaumatoporella*, a micro-problematicum (incertae sedis) with calcareous test, and/or *Decastronema kotori*. Ostracod shells together with small peloids are common. Small benthic foraminifers are also present even if rarely. This facies shows, in place, parallel lamination, dissolution cavities and bird-eyes. The depositional setting was probably the intertidal zone of a tidal flat, also considering the affinity between *Decastronema* and the modern cyanobacterial genus *Scytonema* inhabiting the intertidal flat of Andros island (Golubic et al., 2006)

LF2b: *Thaumatoporella*-foraminiferal wackestone to bindstone. This facies is dominated by *Thaumatoporella* and subordinate benthic foraminifers. Rudists and undetermined bivalves fragments as well as sponge nodules are rare. Non-skeletal grains are represented by abundant micritized grains. This facies is, often, slightly argillaceous and shows faint parallel lamination with *Thaumatoporella* thalli (often strongly compacted) aligned parallel to bedding. Dissolution seams are common. The possible depositional setting of this facies is a restricted intertidal to very shallow subtidal lagoon.

LF3: ostracod-miliolid mudstone-wackestone. This lithofacies occurs in beds 15–40 cm thick beds. It is characterized by ostracods, miliolids and, subordinately, other small benthic foraminifers and *Thaumatoporella*. Dissolution cavities and birdseyes are also common. The inferred depositional setting is intertidal to low-energy shallow subtidal lagoon.

LF4: Foraminiferal wackestone to grainstone. This lithofacies usually overlies LF5 but often can alternate with LF2. It occurs in medium to thick beds (25–50 cm). The main components are represented by small and large sized benthic foraminifers. *Thaumatoporella* algae and bivalve fragments (mainly rudists) are common. Microbial/Sponge and Lithocodium-like nodules, ostracods and *Decastronema* are rare. Dasycladalean algae are common in this facies in the Upper Cenomanian (mainly *Triploporella* and *Russoella*), very rare in the Turonian-Campanian (mainly *Neomeris* and *Salpingoporella*). Among the non-skeletal grains, peloids are abundant to common. The depositional setting of this facies was probably a more or less open subtidal lagoon.

LF5: Rudist packstone-rudstone. This lithofacies occur in medium to very thick beds (20 to >100 cm). It is characterised by mono- to oligospecific assemblages of radiolitic rudists. The matrix of the floatstone and rudstone range from bioclastic wackestone to packstone made of small fragments of rudists and foraminifers. Other bioclasts are represented by rare fragments of ostreids and *Thaumatoporella*. Peloids are common. Rudist fragments are frequently encrusted by *Lithocodium*. The depositional setting of this facies was probably a subtidal open lagoon.

4.1.1. Mt. Varchera

This section is exposed on the south-west slope of Monte Varchera, about 7 km south-east of Sanza, (Fig. 2). We sampled a 250 m thick succession starting ~2 m below the FO of *Cisalveolina fraasi*. Based on the sedimentological and lithological characters the section can be subdivided into four intervals (A–D, fig. 4).

Interval A (0–24 m) starts with a 1 m-thick rudist floatstone (LF5), followed by 13 m of bioclastic mudstones-wackestones and subordinately wackestones-packstones (LF3–4). A dense network of selectively dolomitized *Thalassinoides* burrows characterizes the

first 6.5 m. The bioclasts include larger foraminifers, small benthic foraminifers (mainly miliolids), rudists, ostreids and thin-shelled bivalve fragments. These levels are overlain by 10 m of packstones to floatstones with radiolitic and ostreids (LF 5). Rare foraminiferal wackestones (LF4) also occur. The first part of this interval (0–12 m) contains rich and diverse larger foraminiferal assemblages consisting of *Cisalveolina fraasi*, *Chrysalidina gradata* D'Orbigny, *Pseudolituonella reicheli* Marie, *Biconcava bentori* Hamaoui and Saint-Marc, *Vidalina radoicicae* Cherchi and Schroeder, *Coxites zubairensis* Smout, *Trochospira avnimelechi* Hamaoui and Saint-Marc, *Pseudorhapydionina dubia* (De Castro), *Pseudorhapydionina casertana* (De Castro), *Nezzazata* spp., *Trocholina* sp., *Broeckina* sp., *Dicyclina* sp., *Rotalia* sp. Then, the diversity is sharply reduced leaving an assemblage consisting mainly of *Chrysalidina gradata*, *Pseudolituonella reicheli* and *Pseudorhapydionina dubia*. The larger foraminiferal content allows to refer the first part of this interval to the *Chrysalidina gradata* – *Cisalveolina fraasi* biozone of De Castro (1991) and to the equivalent *Chrysalidina gradata* – *Pseudolituonella reicheli* zone of Chiocchini et al. (2008) (Fig. 1).

Interval B (24–73 m) consists, at the base, of thin-bedded mudstones-wackestones (LF3), often laminated, with small benthic foraminifers ostracods and discorids and less abundant rudists and other undetermined bivalve fragments. This facies (LF3) from 8 m above the base of the interval, becomes regularly alternated with fine-grained *Thaumatoporella*-foraminiferal packstones-grainstones (LF2b) and rare foraminiferal wackestone-packstone (LF4). Fenestrae and dissolution vugs are common in the laminated mudstones-wackestones that are often characterized by brecciated, pseudo-nodular or dolomitized bed tops. The last 20 m of interval B are mainly made of mudstones-wackestones (LF3), passing toward the end of the interval to wackestones and packstones with benthic foraminifers, *Thaumatoporella* and peloids (LF2b) and rare levels of foraminiferal limestones (LF4). The microfossil content of this interval is very scarce in the lower part, where only small benthic foraminifers are found (litolids, miliolids, textularids, *Nezzazinella* sp.). In the middle-upper part benthic foraminifers become more diverse and abundant, with the appearance of *Moncharmontia apenninica* (De Castro), *Reticulinella kaeveri* Cherchi, Radoičic and Schroeder, *Pseudocyclammina sphaeroidea* Gendrot, *Scandonea samnitica* De Castro, *Rotorbinella scarsellai* Torre. Based on its benthic foraminiferal associations, this interval can be referred to the *Pseudocyclammina* spp. zone of De Castro (1991), corresponding to the *Nezzazinella* cf. *aegyptiaca*-*Nummuloculina* cf. *irregularis* zone of Chiocchini et al. (2008) (Fig. 1).

Interval C (73–220 m) consists of abundant rudist floatstones (LF5), alternating with *Thaumatoporella*-*Decastronema* mudstones-wackestones and bindstones (LF2a) and foraminiferal-peloidal packstones to grainstones (LF4). The rudist-rich beds are thicker and more frequent in the middle part of the interval. They consist of dense accumulations of radiolitic shells and fragments. The benthic foraminifers assemblages consist of: *M. apenninica*, *S. samnitica*, *Accordiella conica* Farinacci, *Nezzazinella* sp., *Dicyclina schlumbergeri* Munier-Chalmas, *R. scarsellai*, *P. sphaeroidea*.

Interval D (220–250 m) is mainly made of thin-bedded, often laminated, mudstones-wackestones with *Thaumatoporella* and *Decastronema kotori* (LF2a). More rarely foraminiferal wackestones and packstones of LF4 are also found. Among the benthic foraminifers we identified: *M. apenninica*, *S. samnitica*, *A. conica*, *D. schlumbergeri*, *R. scarsellai*, *P. sphaeroidea*. Based on the microfossils content, intervals C and D can be referred to the *Accordiella conica*-*Moncharmontia apenninica* zone of De Castro (1991) and to the equivalent *Accordiella conica*-*Rotorbinella scarsellai* zone of Chiocchini et al. (2008) (Fig. 1).

4.1.2. Mt. Coccovello

The studied succession crops out on the southern slope of Monte Coccovello, near Maratea (Fig. 2) and consists of ~460 m of Upper Cretaceous shallow-water carbonates. The section was logged from ~50 m below the FO of *C. fraasi* to the top of the Radiolitid Limestones Fm., which coincides with the base of the Paleocene-Eocene limestones and marls of the Trentinara Fm. It has been subdivided into three intervals (A–C, fig. 5).

Interval A (0–73.5 m) consists in the first 50 m of laminated mudstones-wackestones with miliolids and ostracods (LF3), alternating with foraminiferal wackestones-packstones (LF4) and to dolomite beds, often brecciated. Evidence of subaerial exposure is frequent. The last 23 m of the interval are made of 8 m of bioturbated foraminiferal wackestones-packstones (LF4) with dolomite-filled *Thalassinoides* burrows, followed by 10 m of wackestones to floatstones with very thin fragments of rudists and ostraoid shells (LF5) and 5 m of mudstones-wackestones with miliolids and benthic foraminifers (LF3 and rarely LF4). The larger foraminifera of this interval are represented by: *Cisalveolina fraasi*, *Chrysalidina gradata*, *Pseudolituonella reicheli*, *Biconcava bentori*, *Vidalina radoicicae*, *Coxites zubairensis*, *Trochospira avnimelechi*, *Pseudorhapydionina dubia*, *Pseudorhapydionina casertana*, *Nezzazata spp.*, *Trocholina sp.*, *Broeckina sp.*, *Dicyclina sp.*, *Rotalia sp.* Like at Mt. Varchera the biotic diversity is reduced in the last 15 m of the interval where, among larger foraminifers, only *Chrysalidina gradata*, *Pseudolituonella reicheli* and *Pseudorhapydionina dubia* are present. The upper 23 m of this interval can be referred to *Chrysalidina gradata* – *Cisalveolina fraasi* biozone of De Castro (1991) and to the equivalent to the *Chrysalidina gradata* – *Pseudolituonella reicheli* zone of Chiocchini et al. (2008) (Fig. 1).

Interval B (73.5–155 m) consists in the first 20 m mainly of *Thaumatoporella* and ostracod mudstones-wackestones (LF2a) alternating in the lower part with laminated mudstones-wackestones with birdseyes, discorbids and small miliolids (LF3) and in the upper part with foraminiferal-peloidal wackestones-packstones (LF4). Laterally discontinuous m-thick levels of dolomitised intraclastic breccias occur in the middle part of this interval. Foraminiferal associations are generally very poor. The most significant species are *Nezzazatinella sp.*, which is present from the base of the interval, *M. apenninica*, *P. sphaeroidea*, *R. kaeveri* and *S. samnitica* occurring few metres above, and *R. scarsellai*, appearing in the upper part of the interval. According to the microfossil content, this interval can be referred to the “*Pseudocyclamina spp.*” zone of De Castro (1991), corresponding to the *Nezzazatinella cf. aegyptiaca* – *Nummuloculina cf. irregularis* zone of Chiocchini et al. (2008) (Fig. 1).

Interval C (155–450 m) consists mainly of rudist-rich limestones (packstones, floatstones and rudstones; LF5) alternating mainly with laminated mudstones-wackestones and bindstones with *Thaumatoporella*, *Decastronema kotori* and small peloids (LF2a). Rare foraminiferal-peloidal wackestone-packstones (more rarely grainstones) of lithofacies LF4 also occur. From 340 m to 400 m distinct levels of LF1 occur frequently, capping LF2 beds which often show dissolution vugs. The benthic foraminiferal associations of this interval comprise: *D. schlumbergeri*, *M. apenninica*, *P. sphaeroidea*, *Murgella lata* Luperto Sinni, *R. scarsellai*, *A. conica*, *S. samnitica*, *Scandonea mediterranea* De Castro, *Reticulinella fleuryi* Cvetko, Gusic and Schroeder, *Siphodinarella costata* Schlagintweit, Husinec and Jez. Based on its microfossil content, this interval can be referred to *Accordiella conica-Moncharmontia apenninica* zone of De Castro (1991), corresponding to the *Accordiella conica-Rotorbinella scarsellai* zone of Chiocchini et al. (2008) (Fig. 1).

4.1.3. Trentinara

This section has been sampled along two adjacent road cuts of the provincial roads SP113 and SP83, near the village of Trentinara

(Fig. 2). The studied succession is 300 m thick and is entirely referable to the Radiolitid Limestone Fm. (Fig. 6). Three intervals can be distinguished.

Interval A (0–145 m). It is mainly made of laminated wackestones-packstones and bindstones with *Thaumatoporella*, *Decastronema*, microbial/sponge nodules, small benthic foraminifers and ostracods (LF2a–b). Thin beds of rudist packstones to floatstones (LF5) and foraminiferal-bioclastic wackestone-packstone (LF4) are locally intercalated in the first 80–100 m. The last 25 m of the interval are characterized by the presence of distinct, closely spaced levels of characean-ostracod mudstone (LF1). The benthic foraminifers of this interval are represented by: *D. schlumbergeri*, *M. apenninica*, *P. sphaeroidea*, *M. lata*, *R. scarsellai*, *A. conica*, *S. samnitica*, *R. fleuryi*, *S. mediterranea*, *S. costata*, *Nezzazatinella sp.*

Interval B (145–240 m). Here the abundance and thickness of rudist-rich levels (LF5) increase drastically. They are intercalated with mudstones to packstones with *Thaumatoporella*, small benthic foraminifers, *Decastronema*, microbial/sponge nodules, ostracods and with foraminiferal-*Thaumatoporella* wackestones to grainstones (LF2a–b and LF4). The foraminiferal content is similar to that in interval A except for the last 10 m, where *Keramosphaerina tergestina* (Stache) and *Calveziconus cf. lcalveziae* Caus and Cornella have their first appearance.

Interval C (240–297 m). This part of the section records a decrease in the abundance and thickness of rudist levels. It is mainly characterized by slightly dolomitized *Thaumatoporella-Decastronema* and *Thaumatoporella*-foraminiferal wackestone-packstone (LF2a–b) alternating with foraminiferal wackestone-packstone (LF4). The top of the section is unconformably overlain by the Trentinara Fm. Based on the microfossils content, the whole succession can be referred to the *Accordiella conica-Moncharmontia apenninica* zone of De Castro (1991), or to the equivalent *Accordiella conica-Rotorbinella scarsellai* zone of Chiocchini et al. (2008) (Fig. 1).

The most important foraminiferal taxa described in the three studied sections are figured in Figs. 7, 8 and 9.

4.2. Carbon isotope stratigraphy

4.2.1. Mt. Varchera

One hundred and seventy-six samples were analysed for the Mt. Varchera section (Fig. 4). The lower part of the curve (0–39 m) shows a pronounced positive excursion, with isotopic values constantly $> +2\text{‰}$ and a peak of $+4.4\text{‰}$ 1 m above the LO of *C. fraasi*. Then, carbon isotope ratios make a very sharp negative excursion with a minimum of -5.1‰ in the middle part of interval B, at a level close to the FO of *M. apenninica* and *P. sphaeroidea*. This is followed by another positive $\delta^{13}\text{C}$ excursion, which peaks at about $+2.8\text{‰}$, before decreasing to pre-excursion values of $+0.5\text{‰}$. The next segment of the curve is marked by a positive trend, with superimposed small scale fluctuations, culminating in a third $\delta^{13}\text{C}$ spike with a maximum value of $+2.7\text{‰}$ in the upper part of the rudist-rich interval C. Above this level the $\delta^{13}\text{C}$ values fluctuate around $+1$ – 2‰ before abruptly decreasing to a minimum of -2.3‰ in the uppermost part of interval C. In the last 45 m of the $\delta^{13}\text{C}$ curve, values oscillate between 0 and $+1.6\text{‰}$ without any definite trend.

4.2.2. Mt. Coccovello

Three hundred and eleven samples were analysed for the Mt. Coccovello section (Fig. 5). The first 115 m of the $\delta^{13}\text{C}$ profile have been already described in greater detail elsewhere (Parente et al., 2007). The isotopic curve starts with a ~40 m thick interval of fluctuating and mainly negative $\delta^{13}\text{C}$ values. This is followed by a marked positive excursion, which peaks at $+5.4\text{‰}$ in the lowermost part of

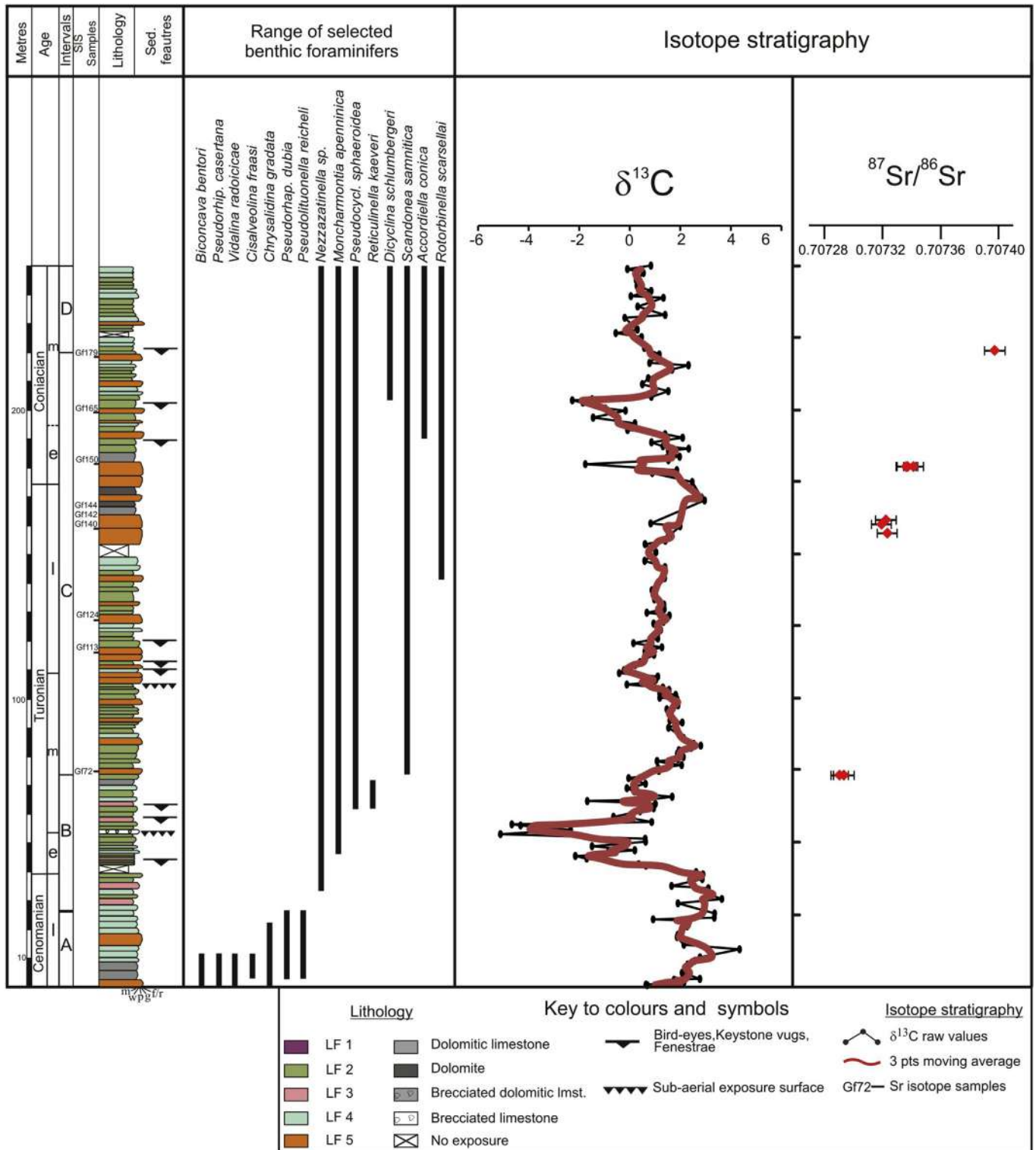


Fig. 4. Lithological–sedimentological log, biostratigraphy, isotope stratigraphy and chronostratigraphy of the Mt. Varchera section. The thick curve represents the 3-point moving average of C-isotope ratios. The chronostratigraphic calibration is constrained by Sr isotope stratigraphy and carbon isotope correlation with the well dated reference curve of [Jarvis et al. \(2006\)](#).

interval B, just above the LO of *P. dubia*. From this level the isotopic values decrease to a minimum of -1.1‰ in the middle part of interval B. A second prominent positive excursion starts close to the FO of *R. kaeveri*, peaking at $+2.8\text{‰}$ at about 120 m from the base of the section. This is followed by a plateau, with values between $+1$

and $+2\text{‰}$, which characterizes the upper part of interval B and the lowermost part of interval C. A third prominent positive excursion covers the next 15 m of the $\delta^{13}C$ curve, peaking at $+4.1\text{‰}$ at ~ 188 m from the base. Over the next ~ 100 m the isotopic curve shows an oscillating trend with values between 0.6 and 2.8‰. The only

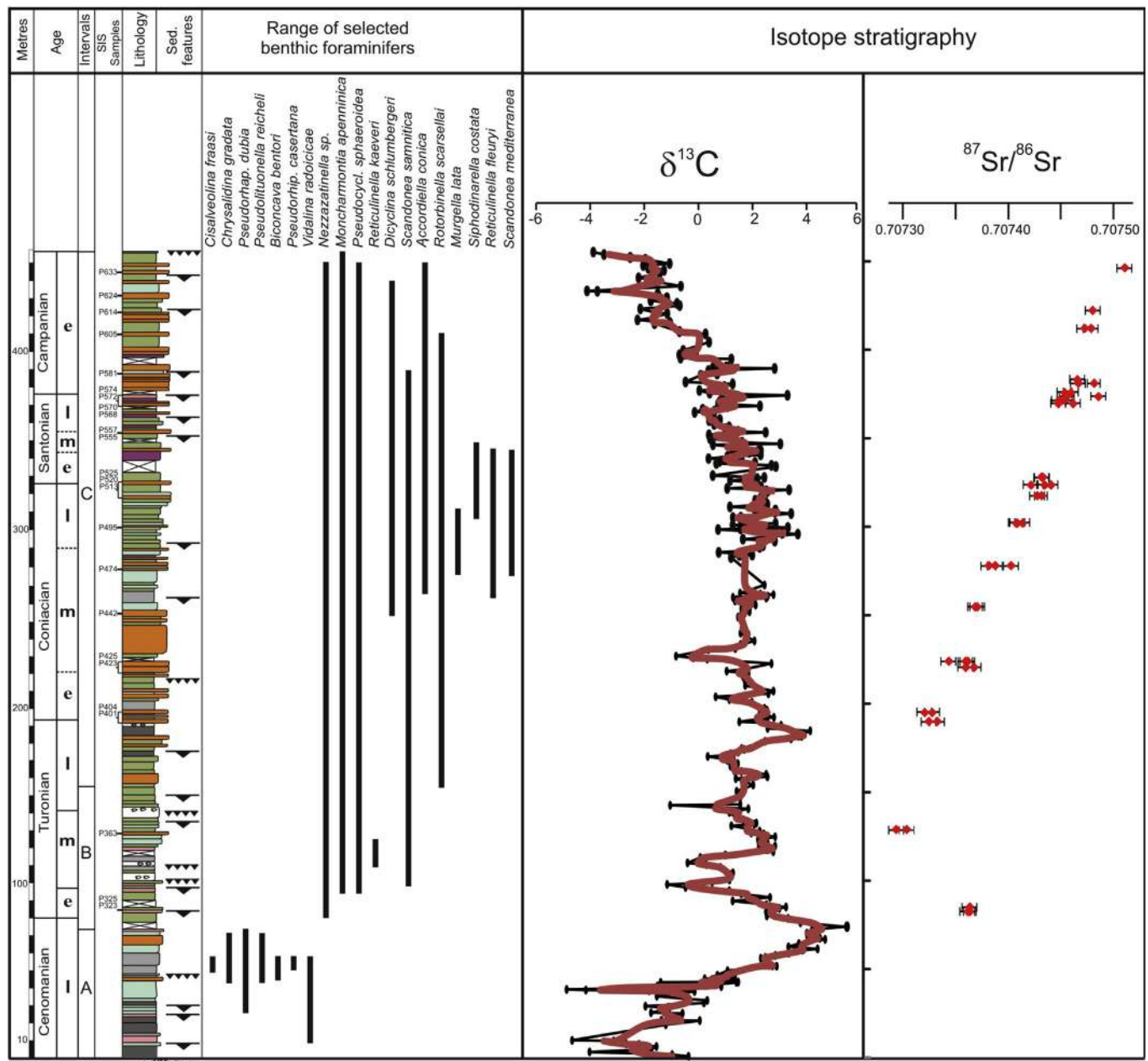


Fig. 5. Lithological–sedimentological log, biostratigraphy, isotope stratigraphy and chronostratigraphy of the Mt. Coccovello section. The thick curve represents the 3-point moving average of C-isotope ratios. The chronostratigraphic calibration is constrained by Sr isotope stratigraphy and carbon isotope correlation with the well dated reference curve of Jarvis et al. (2006). See Fig. 4 for legend.

remarkable event is a negative spike, reaching -0.83‰ , in the middle part of the interval C. In the upper part of interval C, from the FO of *A. conica* and until the end of the section, the $\delta^{13}\text{C}$ profile shows a general decreasing trend with superimposed minor oscillations. The last 50 m of the curve show negative $\delta^{13}\text{C}$ values, mainly fluctuating between -0.7 and -2.3‰ , except for the last 30 m where values as negative as -4.1‰ are found.

4.2.3. Trentinara

Two hundred and fifty-eight samples were analysed for the Trentinara section (Fig. 6). The first 100 m of the isotopic profile do not show any prominent trend or event. This part of the curve is characterised by values oscillating mainly between $+0.5$ and 2.5‰ , except in its middle part, where an interval with more negative

values is present. Then, the $\delta^{13}\text{C}$ values start increasing; they reach a maximum of $+3\text{‰}$ at about 120 m from the base and abruptly decrease to -1.2‰ just before the first level with *M. lata*. The next 27 m of the $\delta^{13}\text{C}$ profile are characterized by high amplitude fluctuations around a mean value of 1‰ without any definite trend. Above this interval there is a prominent positive excursion starting from isotopic values around 0‰ , peaking with values between $+2.2$ and $+3.2\text{‰}$ that make a plateau of ~ 30 m, before returning to the pre-excursion values at around 200 m from the base of the section. This positive C-isotope event is followed by a general decreasing trend characterized by high amplitude fluctuations of around 3‰ . The last 13 m of the $\delta^{13}\text{C}$ profile show an abrupt drop of the isotopic values from $+0.5$ to -6.7‰ just below the contact with the Trentinara Fm.

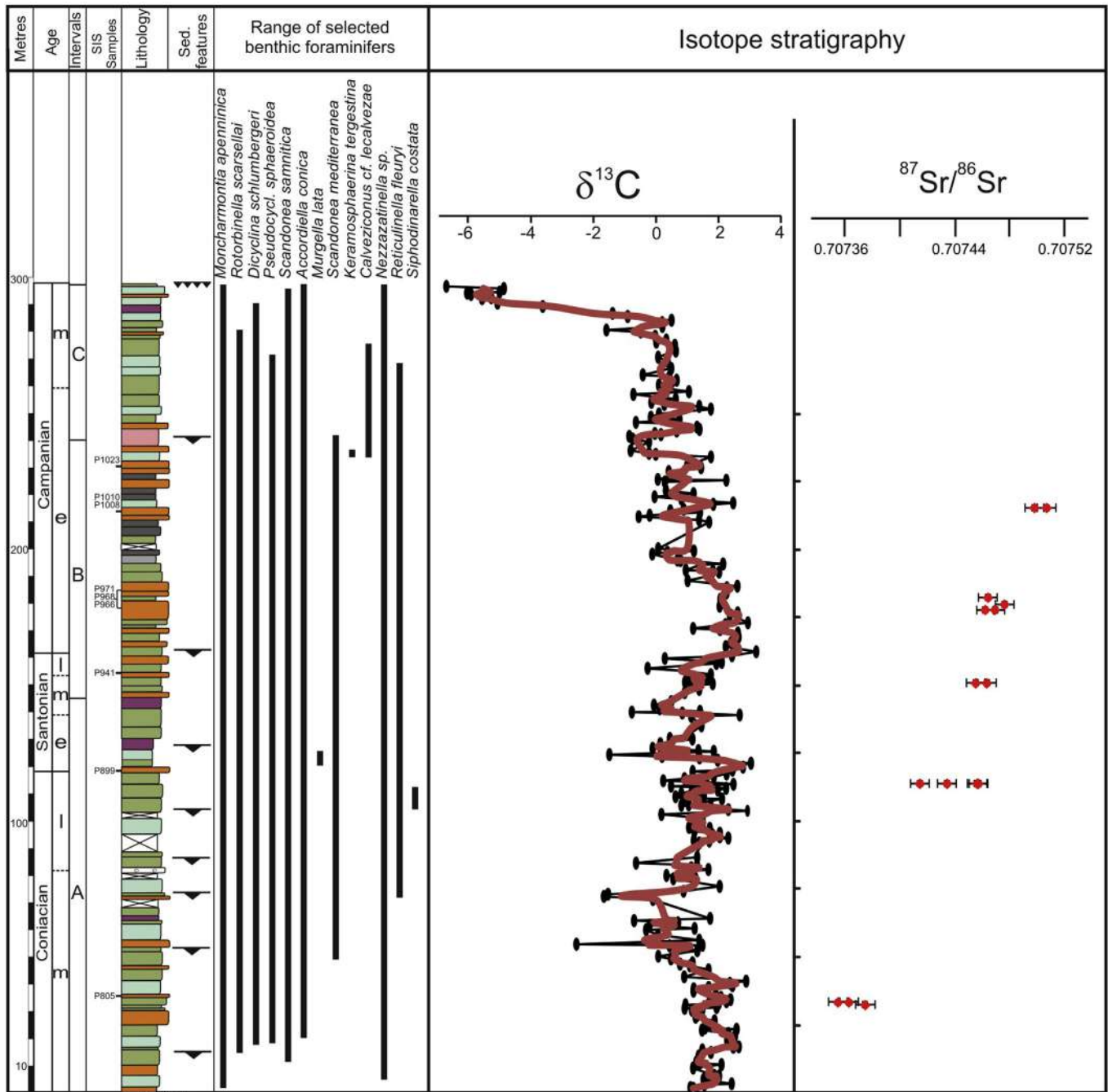


Fig. 6. Lithological–sedimentological log, biostratigraphy, isotope stratigraphy and chronostratigraphy of Trentinara section. The thick curve represents the 3-point moving average of C-isotope ratios. The chronostratigraphic calibration is constrained by Sr isotope stratigraphy and carbon isotope correlation with the well dated reference curve of [Jarvis et al. \(2006\)](#). See [Fig. 4](#) for legend.

4.3. Sr-isotope stratigraphy

The late Cenomanian–Maastrichtian (93.05 ± 0.2 – 65.0 ± 0.1 Ma; [Gradstein et al., 2004](#)) portion of the marine strontium isotope reference curve ([McArthur et al., 2001](#); [McArthur and Howarth, 2004](#)) is derived from the Chalk of southern England ([McArthur et al., 1993](#)) and from the Western Interior Seaway ([McArthur et al., 1994](#)). In this interval, the curve is characterized by two steep segments, a descending branch in the latest Cenomanian–middle Turonian and an ascending branch in the latest Turonian–

Maastrichtian, separated by a turning point with the lowest values in the late Turonian. The very narrow half-width of the 95% confidence intervals on the estimated $^{87}\text{Sr}/^{86}\text{Sr}$ value (about ± 0.000004), combined with the high slope of the curve on both sides of the late Turonian minimum, allows for a potential maximum precision of ± 200 – 700 kyr in Turonian–Maastrichtian successions ([McArthur et al., 2001](#)). These characteristics make the Late Cretaceous one of the most favourable interval for high resolution dating and correlation of marine carbonates with SIS.

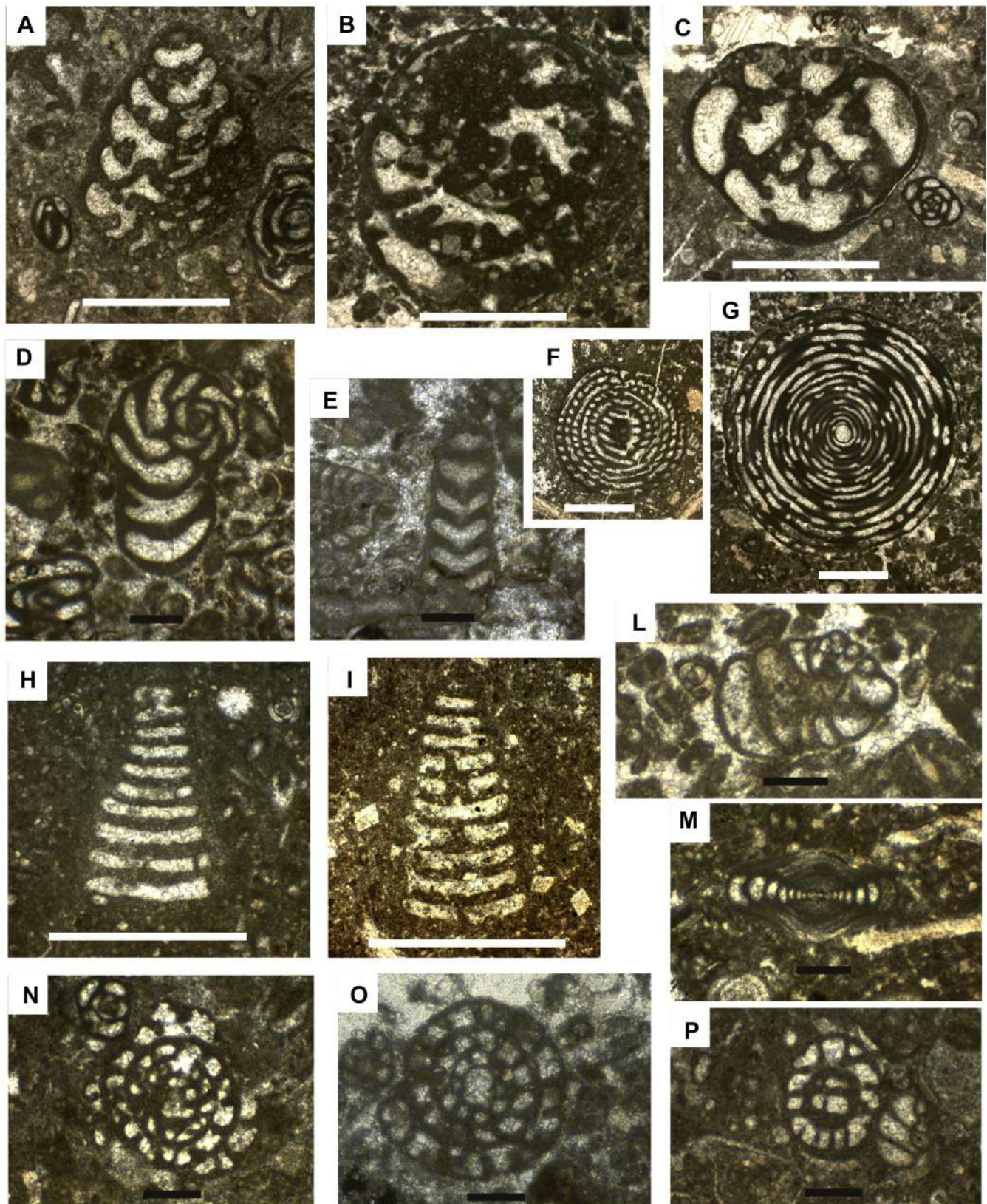


Fig. 7. Selected benthic foraminifers from the Cenomanian-Turonian interval of the studied sections. **A–C** *Crhyssalidina gradata* (a and c: P314, Mt. Coccovello, b: GF 14, Mt. Varchera); **D–E** *Pseudorhapydionina dubia* (P298, Mt. Coccovello); **F–G** *Cisalveolina fraasi* (f: GF19 and g: GF14, Mt. Varchera); **H–I** *Pseudolituonella reicheli* (h: GF14 and i: GF15, Mt. Varchera); **L** *Nezzazatinella* sp. (corresponding to *N. cf. aegyptiaca* of [Chiocchini et al., 2008](#)) (P324, Mt. Coccovello); **M** *Vidalina radoicicae* (GF17, Mt. Varchera); **N–P** *Reticulinella kaeveri* (n and p: GF 66, Mt. Varchera, o: P352, Mt. Coccovello). White scale bar = 1 mm, Black scale bar = 200 μm.

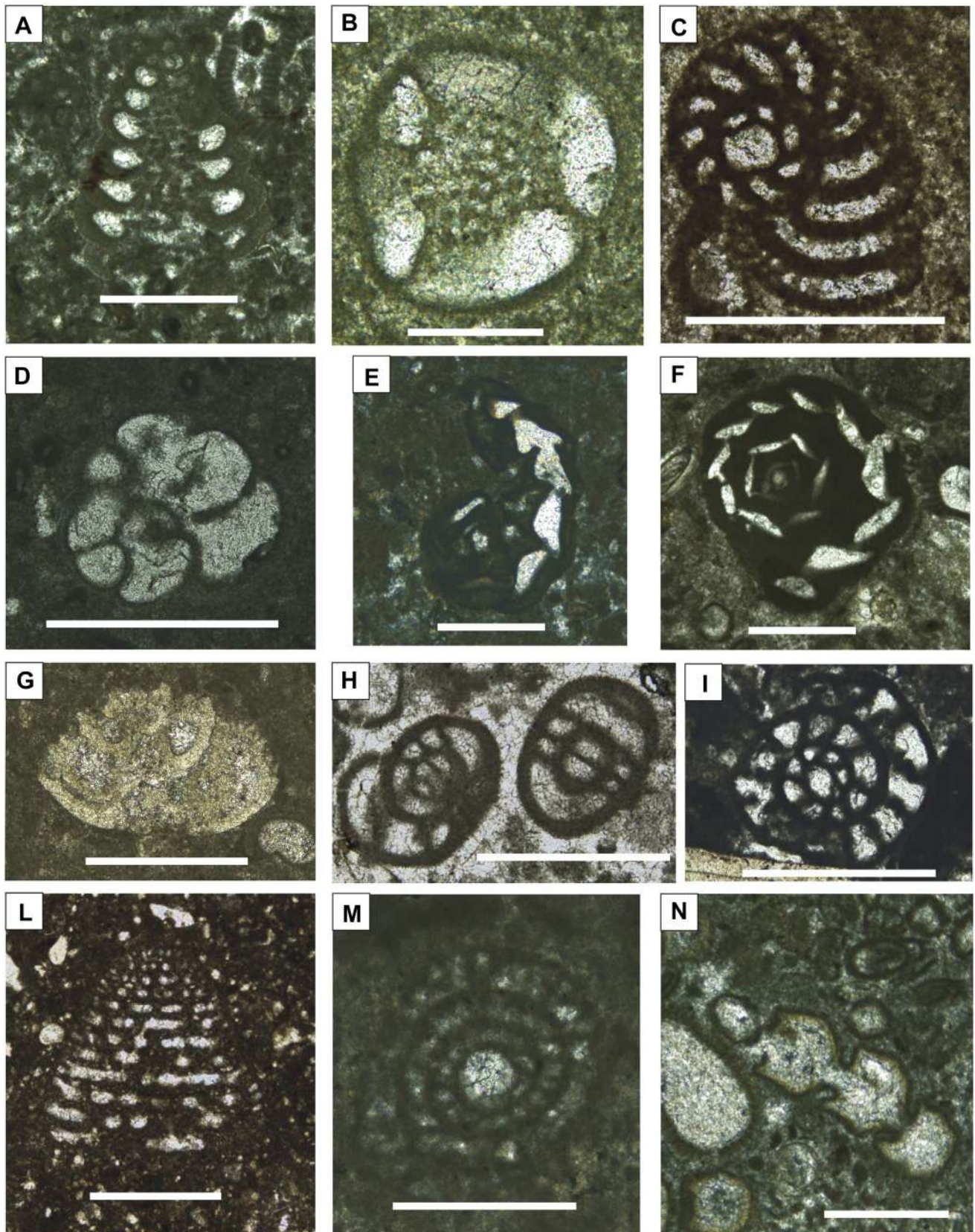


Fig. 8. Selected benthic foraminifers from the Turonian-Campanian interval of the studied sections. **A–B** *Accordiella conica* (a: P 934 and b: P 1044, Trentinara); **C** *Pseudocyclammina sphaeroidea* (P 871, Trentinara); **D** *Nezzazatinella* sp. (corresponding to *N. cf. aegyptiaca* of [Chiocchini et al., 2008](#)) (P 933, Trentinara); **E–F** *Scandonea samnitica* (c: P 793 and d: P 1033, Trentinara); **G** *Rotorbinella scarsellai* (P 1043, Trentinara); **H–I** *Moncharmontia apenninica* (h: P 1078 and i: P 1060, Trentinara); **L** *Calveziconus cf. lecalvezae* (P 1027, Trentinara); **M** *Reticulinella fleuryi* (P 1057, Trentinara); **N** *Siphodinarella costata* (P 882, Trentinara). White scale bar = 200 μm, Black scale bar = 100 μm.

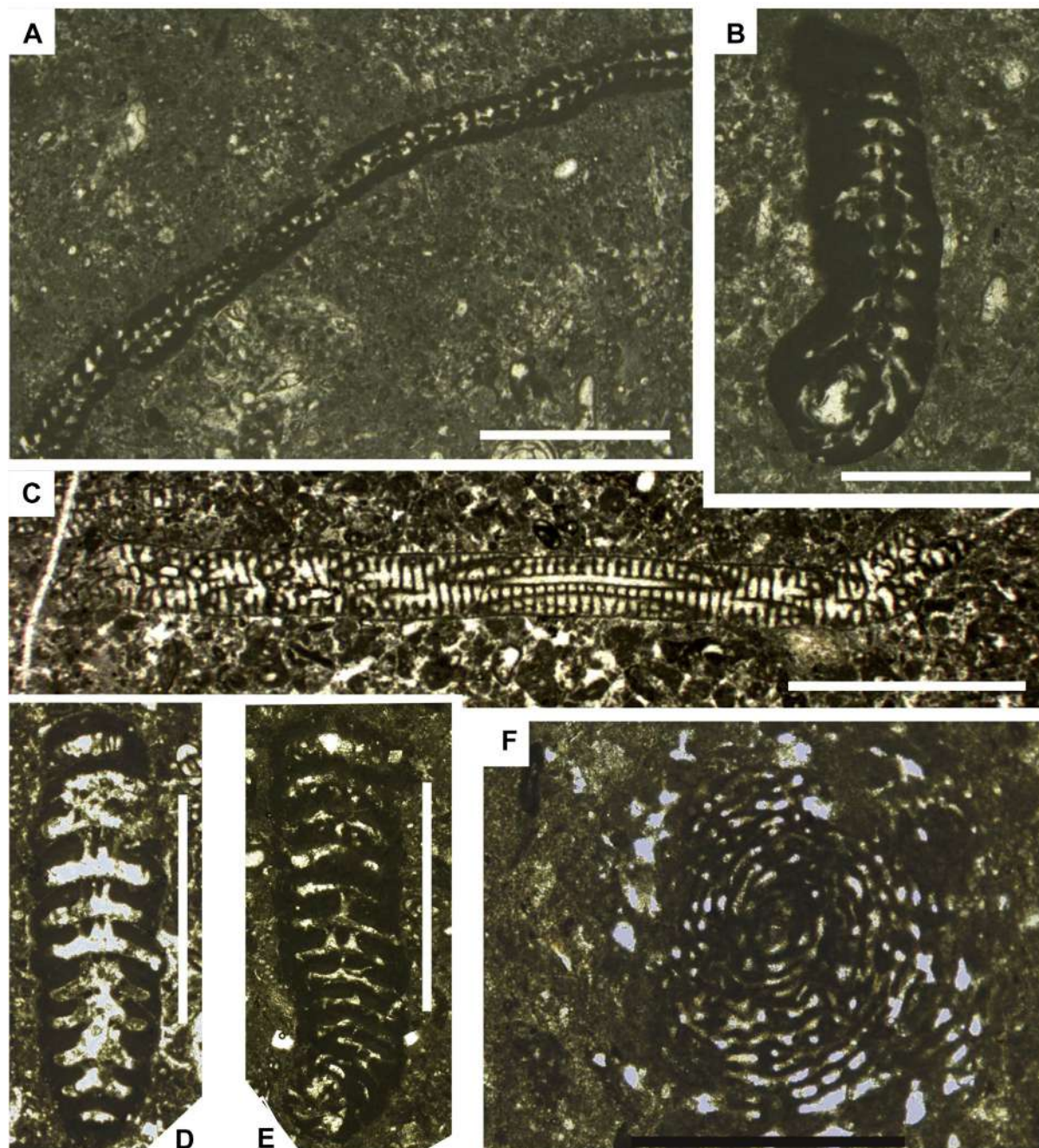


Fig. 9. Selected benthic foraminifers from the Coniacian-Campanian interval of the studied sections. **A–B** *Murgella lata* (P 915, Trentinara); **C** *Dicyclina schlumbergeri* (P 818, Trentinara); **D–E** *Scandonea mediterranea* (d: P 1022 and e: p 1035, Trentinara); **F** *Keramospaerina tergestina* (P 1028, Trentinara). White scale bar = 2 mm, Black scale bar = 1 mm.

4.3.1. Evaluating the preservation of samples

The first step, when using marine carbonates for SIS, is to carefully evaluate the degree of preservation of the samples. In fact, only marine precipitates that have retained the original Sr-isotope ratio of the ocean will give correct SIS ages. Many studies proved that the low-Mg biotic calcite of bivalve shells, and especially of rudists, is one of the most suitable material for Cretaceous carbonates (Steuber, 2001, 2003; Steuber et al., 2005; Frijia and Parente, 2008a,b; Steuber and Schlüter, 2012; Boix et al., 2011; Vicedo et al., 2011; Caus et al., 2013; Huck et al., 2013; Albrich et al., 2014). Samples showing a good preservation of the original shell microstructure have the best chance to have retained their original

Sr-isotope ratio. Petrographic observations with the optical microscope (under polarized light and cathodoluminescence) and SEM show an excellent preservation of the prismatic microstructure of the shell for most of the samples of rudist shells analysed for this work. Only in a limited number of samples we found evidence of alteration, highlighted by partially fused or micritized calcite prisms (Fig. 10). Analysis of the concentration of some major and trace elements is also a powerful tool to estimate the degree of alteration of a sample of biotic calcite. Diagenesis usually proceeds by decreasing Sr concentration and increasing Fe and Mn concentrations (Brand and Veizer, 1980; Al-Aasm and Veizer, 1986; Brand et al., 2012). However, in some case studies, low Fe and Mn concentrations have

been found also in diagenetic calcite (Steuber et al., 2005; Frijia and Parente, 2008a,b; Boix et al., 2011; Vicedo et al., 2011), suggesting that diagenetic fluids are not necessarily enriched in Fe and Mn. In fact, solubility of Mn and Fe predominantly depends on the redox potential of diagenetic fluids. Most of the rudist samples analysed for this study have low Fe and Mn concentrations (Table 1 and Fig. 11), below the thresholds used by different authors to discriminate well preserved material (Steuber, 1999; Steuber et al., 2002, 2005; Huck et al., 2011). Furthermore, our samples do not show any clear diagenetic trend of increasing Fe and/or Mn with decreasing Sr concentration (Fig. 11). Shells with well preserved pristine microstructure and high Sr content show, in some cases, higher Fe concentration than samples with petrographic evidence of recrystallization and low Sr concentration. Therefore, we did not use Fe and Mn concentration as the prime criterion of diagenetic screening and relied mainly on Sr concentration. Most of the shells retaining the pristine microstructure show a Sr concentration >1000 ppm, which is the mean value of Sr concentration in modern brachiopods and bivalves (Al-Aasm and Veizer, 1986; Carpenter and Lohmann, 1992). However, for our dataset we used a cut-off limit of 750 ppm, which is slightly below the 800 ppm threshold adopted by Steuber et al. (2005) in their study on the Upper Cretaceous platform carbonates of the island of Brač (Croatia). Samples with a Sr concentration above this limit where used for SIS, but only if they also passed the petrographic screening of pristine microstructure preservation (Table 1 and Fig. 11).

The next step of our diagenetic screening procedure was to compare the Sr concentration and the Sr-isotope value of different rudist shells (with different degree of preservation) and different components (rudists, matrix, cements) from the same level. Our data show that late diagenetic cements, micritic matrix and poorly preserved rudist shells have lower Sr concentration and higher Sr-isotope values than pristine shells. This is the trend expected for diagenetic alteration or for mixing of pristine and diagenetic material (Banner, 1995). For this reason, when a set of well preserved shells from the same level showed a scatter in Sr isotope ratios $>20 \times 10^{-6}$, we discarded the sample with the highest $^{87}\text{Sr}/^{86}\text{Sr}$ value (i.e. P582B, P614G-F, see Table 1). In our dataset, these enigmatic outliers are very rare. With very few exceptions, shells from the same bed, which passed all the steps of our diagenetic screening procedure, have $^{87}\text{Sr}/^{86}\text{Sr}$ values within the limits of the analytical precision ($2 \text{ s.e.} = \pm 7 \times 10^{-6}$). This coherence and concordance of data can be considered as strong evidence that the samples we used for SIS retained their original marine Sr-isotope signature (McArthur, 1994; McArthur et al., 2006; Brand et al., 2011).

4.3.2. Mt. Coccovello

At Mt. Coccovello we collected for SIS 54 samples from 25 different stratigraphic levels. The average spacing was 15 m in the Radiolitic Limestones Fm. The $^{87}\text{Sr}/^{86}\text{Sr}$ mean value of bivalve samples just above the end of the largest C-isotope positive excursion of the $\delta^{13}\text{C}$ curve gives an age of 93.44 Ma, corresponding

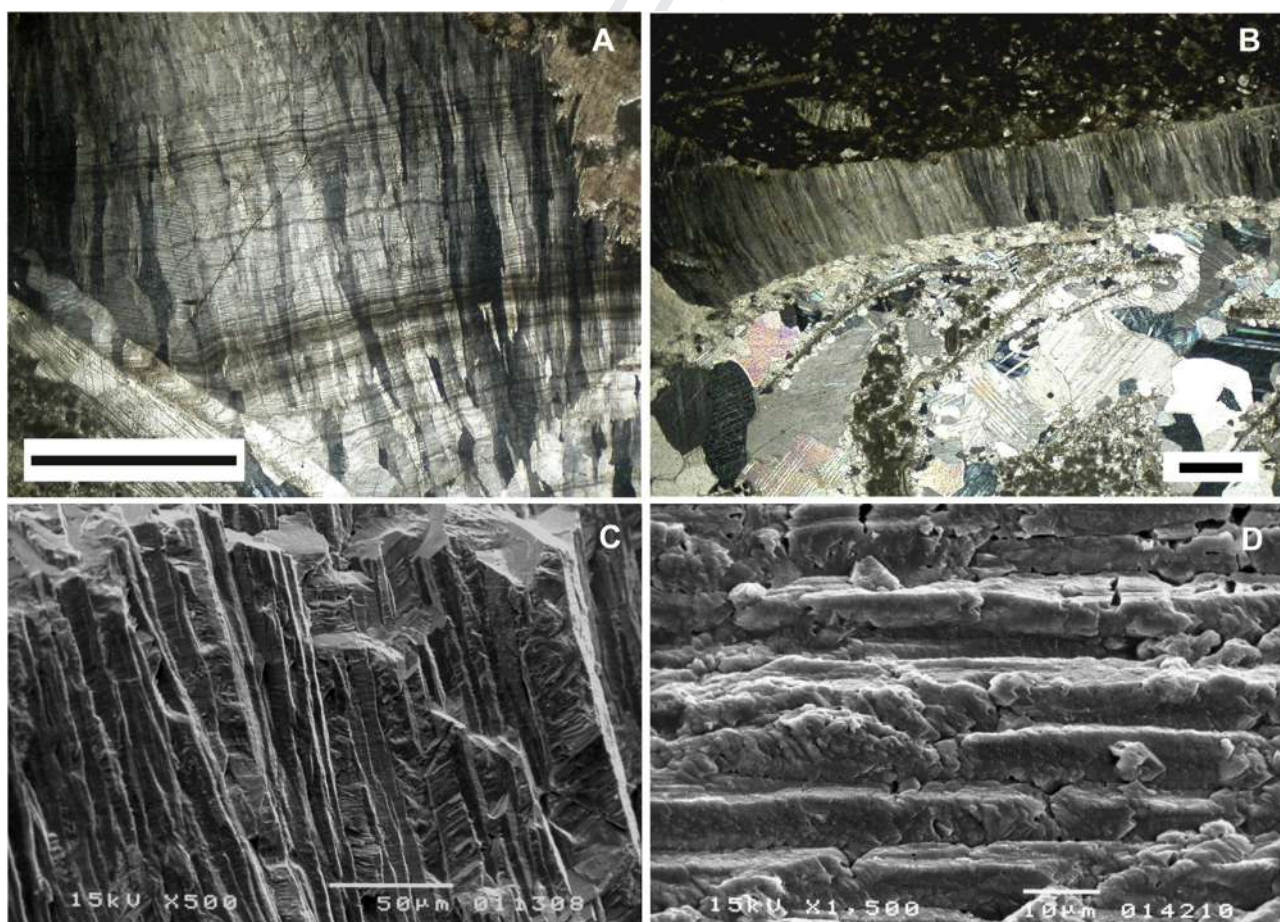


Fig. 10. Thin section (A–B) and SEM (C–D) photomicrographs of rudist shells. A–B compact portion of the outer shell layer of two different rudist shells, showing a well preserved prismatic structure; growth lines are evident in A (crossed nicols, scale bar = 500 μm) (a: GF140, Mt. Varchera and b: P 301, Mt. Coccovello); C SEM photomicrograph showing the original prismatic ultrastructure of a rudist shell (GF 113, Mt. varchera); D SEM photomicrograph showing a rudist shells whose original microstructure has been partially altered by diagenesis. Note the partially fused and micritized calcite prisms (GF 142, Mt. varchera).

Table 1
Elemental and isotopic composition of biotic calcite, micrite and cement from the studied sections.

Sample	Component	Section	Mg (ppm)	Sr (ppm)	Fe (ppm)	Mn (ppm)	⁸⁷ Sr/ ⁸⁶ Sr	2 s.e. (*10 ⁻⁶)	Preservation
P323 A1a	Undet. bivalve	Mt. Coccovello	nd	nd	nd	nd	0.707361	7	P
P323 A3a	Undet. bivalve	Mt. Coccovello	nd	nd	nd	nd	0.707363	6	P
P325 A2a	Undet. bivalve	Mt. Coccovello	nd	nd	nd	nd	0.707363	7	P
P 363 A	Rudist	Mt. Coccovello	3608	1155	64	0.5	0.707303	7	P
P 363 B	Rudist	Mt. Coccovello	2589	1193	51	0.5	0.707293	7	P
P 363 M	Matrix	Mt. Coccovello	3849	434	78.8	2.3	0.707336	7	
P401 A	Rudist	Mt. Coccovello	1252	1004	8	0.5	0.707332	7	P
P401 B	Rudist	Mt. Coccovello	1601	876	7	0.5	0.707324	7	P
P404 A	Rudist	Mt. Coccovello	1669	1019	9	0.5	0.707320	7	P
P404 B	Rudist	Mt. Coccovello	1783	996	7	0.5	0.707327	7	P
P423A	Rudist	Mt. Coccovello	2624	1339	15	0.5	0.707359	7	P
P423B	Rudist	Mt. Coccovello	2554	1284	18	0.5	0.707367	7	P
P425A	Rudist	Mt. Coccovello	2076	1491	20	0.5	0.707359	7	P
P425B	Rudist	Mt. Coccovello	1324	1315	43	0.5	0.707361	7	P
P425C	Rudist	Mt. Coccovello	1416	1207	13	0.5	0.707343	7	P
P442A	Rudist	Mt. Coccovello	1162	1197	19	0.5	0.707370	7	P
P442B	Rudist	Mt. Coccovello	1496	1448	14	0.5	0.707368	7	P
P474AA	Rudist	Mt. Coccovello	2030	1738	8	0.5	0.707381	7	P
P474AB	Rudist	Mt. Coccovello	2245	1352	12	0.5	0.707387	7	P
P474AC	Rudist	Mt. Coccovello	3409	1467	5	0.5	0.707402	7	P
P495AA	Rudist	Mt. Coccovello	1347	1241	19	0.5	0.707408	7	P
P495AB	Rudist	Mt. Coccovello	1732	1059	20	0.9	0.707407	7	P
P495AC	Rudist	Mt. Coccovello	1960	1388	16	1.3	0.707413	7	P
P513A	Rudist	Mt. Coccovello	1682	1196	43	0.5	0.707427	7	P
P513C	Rudist	Mt. Coccovello	1537	1551	15	0.5	0.707431	6	P
P520A	Rudist	Mt. Coccovello	1472	2228	12	0.5	0.707434	7	P
P520B	Rudist	Mt. Coccovello	1731	1358	23	0.5	0.707421	7	P
P520C	Rudist	Mt. Coccovello	1716	1256	20	0.5	0.707440	7	P
P525A	Rudist	Mt. Coccovello	1831	1599	10	0.5	0.707431	7	P
P525B	Rudist	Mt. Coccovello	1707	1504	6	0.5	0.707432	7	P
P555	Rudist	Mt. Coccovello	2176	1490	13	0.5	0.707462	7	P
P557	Rudist	Mt. Coccovello	1991	1376	8	0.5	0.707458	7	P
P568A	Rudist	Mt. Coccovello	2112	1164	19	0.5	0.707461	7	P
P568B	Rudist	Mt. Coccovello	2435	1495	75	0.5	0.707447	7	P
P570A	Rudist	Mt. Coccovello	1813	1184	7	0.5	0.707453	7	P
P570B	Rudist	Mt. Coccovello	1937	1318	2	0.5	0.707448	7	P
P572A	Rudist	Mt. Coccovello	2045	1424	17	0.5	0.707485	7	P
P572B	Rudist	Mt. Coccovello	1905	1432	16	0.5	0.707455	7	P
P574A	Rudist	Mt. Coccovello	1994	1421	3	0.5	0.707453	7	P
P574B	Rudist	Mt. Coccovello	2353	1351	35	0.5	0.707459	7	P
P581A	Rudist	Mt. Coccovello	1581	1591	12	0.5	0.707481	6	P
P581B	Rudist	Mt. Coccovello	1984	1631	11	0.5	0.707466	7	P
P582A	Rudist	Mt. Coccovello	1853	1227	14	0.5	0.707465	7	P
P582B	Rudist	Mt. Coccovello	2420	1083	15	0.5	0.707491	7	A
P605A	Rudist	Mt. Coccovello	1195	1253	10	0.5	0.707478	7	P
P605B	Rudist	Mt. Coccovello	1443	1407	4	0.5	0.707472	7	P
P614A	Rudist	Mt. Coccovello	1115	1206	91	3.7	0.707480	7	P
P614B	Rudist	Mt. Coccovello	1059	1237	55	2.1	0.707510	7	A
P614C	Rudist	Mt. Coccovello	1005	1253	111	2.3	0.707530	7	A
P614F	Rudist	Mt. Coccovello	995	271	166	4.4	0.707524	7	A
P624A	Rudist	Mt. Coccovello	941	944	104	2.4	0.707522	7	A
P624B	Rudist	Mt. Coccovello	1151	717	179	5.9	0.707501	7	A
P633A	Rudist	Mt. Coccovello	1874	841	131	16.4	0.707532	7	A
P633C	Rudist	Mt. Coccovello	1323	1160	143	11.5	0.707510	7	P
GF72 B	Rudist	Mt. Varchera	2020	891	9	0.6	0.707290	6	P
GF72 A	Rudist	Mt. Varchera	1552	1063	2	0.5	0.707293	7	P
GF72M	Matrix	Mt. Varchera	2833	205	45	4.0	0.707411	7	
GF113 A	Rudist	Mt. Varchera	1827	764	12	0.5	0.707321	7	A
GF113 M	Matrix	Mt. Varchera	3588	233	99	2.6	0.707381	7	
GF124 B	Rudist	Mt. Varchera	2146	484	9	1.4	0.707316	7	A
GF124 A	Rudist	Mt. Varchera	1734	645	21	1.4	0.707316	7	A
GF124 M	Matrix	Mt. Varchera	2116	164	59	2.7	0.707444	6	
GF140	Rudist	Mt. Varchera	n.d.	n.d.	n.d.	n.d.	0.707323	7	P
GF142 B	Rudist	Mt. Varchera	1901	826	14	0.5	0.707352	7	PA
GF142 A	Rudist	Mt. Varchera	2628	781	13	0.5	0.707319	7	P
GF142M	Matrix	Mt. Varchera	2532	209	96	1.8	0.707436	7	
GF144	Rudist	Mt. Varchera	n.d.	n.d.	n.d.	n.d.	0.707322	7	P
GF149	Rudist	Mt. Varchera	1706	949	89	1.3	0.707468	7	A
GF149 M	Matrix	Mt. Varchera	2743	227	57	2.5	0.707427	7	
GF149 T	Cement	Mt. Varchera	2545	106	18	4	0.707812	7	
GF150 B	Rudist	Mt. Varchera	2482	1030	102	2.0	0.707341	7	P
GF150 A	Rudist	Mt. Varchera	2369	1104	273	2.0	0.707337	7	P
GF150	Rudist	Mt. Varchera	n.d.	n.d.	n.d.	n.d.	0.707336	7	P
GF150 T	Cement	Mt. Varchera	2721	106	11	5	0.707837	7	

Table 1 (continued)

Sample	Component	Section	Mg (ppm)	Sr (ppm)	Fe (ppm)	Mn (ppm)	$^{87}\text{Sr}/^{86}\text{Sr}$	2 s.e. ($\times 10^{-6}$)	Preservation
GF165	Rudist	Mt. Varchera	1647	1127	25	0.5	0.707476	7	A
GF165 M	Matrix	Mt. Varchera	2799	254	95	8.9	0.707455	7	
GF179	Rudist	Mt. Varchera	1507	989	14	0.5	0.707397	7	P
GF179 M	Matrix	Mt. Varchera	3244	229	73	3.1	0.707481	7	
P 805C	Rudist	Trentinara	1315	1125	0.5	0.5	0.707374	7	P
P 808 A	Rudist	Trentinara	1500	1419	69.7	0.8	0.707362	7	P
P 808 C	Rudist	Trentinara	1448	1500	151.9	6.1	0.707354	7	P
P 808 M	Matrix	Trentinara	2764	382	41.7	2.3	0.707431	7	
P 899 A	Rudist	Trentinara	1609	1505	55.2	0.5	0.707457	7	PA
P 899 D	Rudist	Trentinara	1583	1274	57.6	0.5	0.707434	7	P
P 899X	Rudist	Trentinara	2356	877	0.5	1.4	0.707456	7	PA
P 899G	Rudist	Trentinara	1714	1258	0.5	0.5	0.707414	7	P
P 941 A	Rudist	Trentinara	1909	1666	37.3	0.5	0.707463	7	P
P 941 C	Rudist	Trentinara	1718	1518	73.4	0.5	0.707455	7	P
P 941 M	Matrix	Trentinara	3516	310	43.3	2.9	0.707509	7	
P 966X	Rudist	Trentinara	1735	1156	0.5	0.5	0.707469	7	P
P 966 B	Rudist	Trentinara	1397	1461	84.2	0.5	0.707462	6	P
P 966M	Matrix	Trentinara	3167	239	13.2	2.9	0.707531	7	
P 966T	Cement	Trentinara	2597	127	0.5	3.2	0.707743	7	
P 968C	Rudist	Trentinara	1534	987	0.5	0.5	0.707476	7	P
P968T	Cement	Trentinara	2399	139	23.8	1.6	0.707675	7	
P 971A	Rudist	Trentinara	1860	998	0.5	0.5	0.707464	7	P
P 971M	Matrix	Trentinara	3790	227	14.4	1.9	0.707518	6	
P1008A	Rudist	Trentinara	2014	1101	22.0	1	0.707507	7	P
P1008D	Rudist	Trentinara	2642	1103	39.8	0.7	0.7074979598	7	P
P1008M	Matrix	Trentinara	2817	377	82.0	2.8	0.70755	7	
P1010A	Rudist	Trentinara	1459	890	15.8	0.5	0.7075239604	6	PA
P1010M	Matrix	Trentinara	3631	358	71.4	2.7	0.707576	9	
P1023X	Rudist	Trentinara	2115	716	28.8	1.6	0.7075309606	7	A
P1023G	Rudist	Trentinara	2975	447	23.1	2.6	0.7075339607	7	A
P1023M	Matrix	Trentinara	3950	317	61.6	3.1	0.707569	6	

P = preserved, PA = partially altered, A = Altered.

to the early Turonian (Table 2). The positive $\delta^{13}\text{C}$ excursion has been correlated to that occurring worldwide in the Cenomanian-Turonian boundary (CTB) interval (Parente et al., 2007, 2008; Fig. 5 and 13), thus indicating the good agreement between SIS and C-isotope stratigraphy. The next analysed level for SIS comes from the first rudist floatstone found above the end of the positive C-isotope excursion occurring at ~130 m from the base of the section. The mean Sr-isotope value of 0.707298 of this level is the lowest measured for the whole Coccovello section and falls in the late Turonian $^{87}\text{Sr}/^{86}\text{Sr}$ minimum of the reference curve of McArthur et al. (2004). For this isotopic ratio two possible numerical ages are obtained (89.58 and 90.66 Ma), which bracket the middle-late Turonian boundary. From this level until the top of the section the $^{87}\text{Sr}/^{86}\text{Sr}$ values show a regular increasing trend, corresponding to the late Turonian-Maastrichtian segment of the marine reference curve (McArthur et al., 2004). Our densely spaced SIS data allow an accurate chronostratigraphic calibration of the studied section. A level at about 190 m from the base, ~2 m above the last prominent positive C-isotope excursion, has a mean $^{87}\text{Sr}/^{86}\text{Sr}$ value of 0.707326, which translates into a numerical age of 89.04 Ma, corresponding to the Turonian-Coniacian boundary. The $^{87}\text{Sr}/^{86}\text{Sr}$ mean value of 0.747431, obtained from a level at ~323 m from the base of the section, gives an age of 85.65 Ma, which corresponds to the earliest Santonian, very close to the Coniacian-Santonian boundary. Higher up, a level at ~373 m from the base of the section yields a Sr-isotope value of 0.707458, which gives an age of 83.18 Ma, corresponding to the earliest Campanian, very close to the Santonian-Campanian boundary. The highest $^{87}\text{Sr}/^{86}\text{Sr}$ value of 0.707510 has been measured few metres below the unconformity separating the Radiolitic Limestones from the Paleocene-Eocene deposits of the Trentinara Fm. This value translates into an age of 79.90 Ma, which indicates a early-middle Campanian age for the top of the Cretaceous limestones at Mt. Coccovello.

4.3.3. Mt. Varchera

At Mt. Varchera seven rudist levels were sampled but only four of them provided suitable material for SIS (Fig. 4). The first samples come from a rudist floatstone at about 73 m from the base of the section. Their $^{87}\text{Sr}/^{86}\text{Sr}$ mean value of 0.707292 indicates a late Turonian age and is within error from the value obtained at Monte Coccovello from the stratigraphically correlative rudist floatstone. Above this level, which plots in the late Turonian minimum of the marine reference curve, the other SIS samples depict a gradual increase of the $^{87}\text{Sr}/^{86}\text{Sr}$ ratio up to a maximum of 0.707397 found at the top of the section. This value translates into a numerical age of 86.88 Ma, corresponding to the late Coniacian (Table 2).

4.3.4. Trentinara

Six rudist levels were sampled from the Trentinara section (Fig. 6). The last level, just beneath the unconformity separating the Radiolitic Limestones from the Trentinara Fm, did not give suitable material for SIS. The lower part of the section can be dated as middle Coniacian, based on the mean $^{87}\text{Sr}/^{86}\text{Sr}$ value of 0.707363 (87.82 Ma) obtained for a level at about 33 m from the base. Like in the other sections, the $^{87}\text{Sr}/^{86}\text{Sr}$ values increase regularly up-section. The highest $^{87}\text{Sr}/^{86}\text{Sr}$ value (0.707502) has been obtained from a level about 25 m below the base of the Trentinara Fm. This value translates into an age of 80.64 Ma, corresponding to the early Campanian.

5. Discussion

5.1. C-isotope stratigraphy

Carbon-isotope stratigraphy is essentially practiced by matching the patterns (i.e. the isotopic trends and excursions) of the $\delta^{13}\text{C}$ profile retrieved by a succession under study with a reference $\delta^{13}\text{C}$

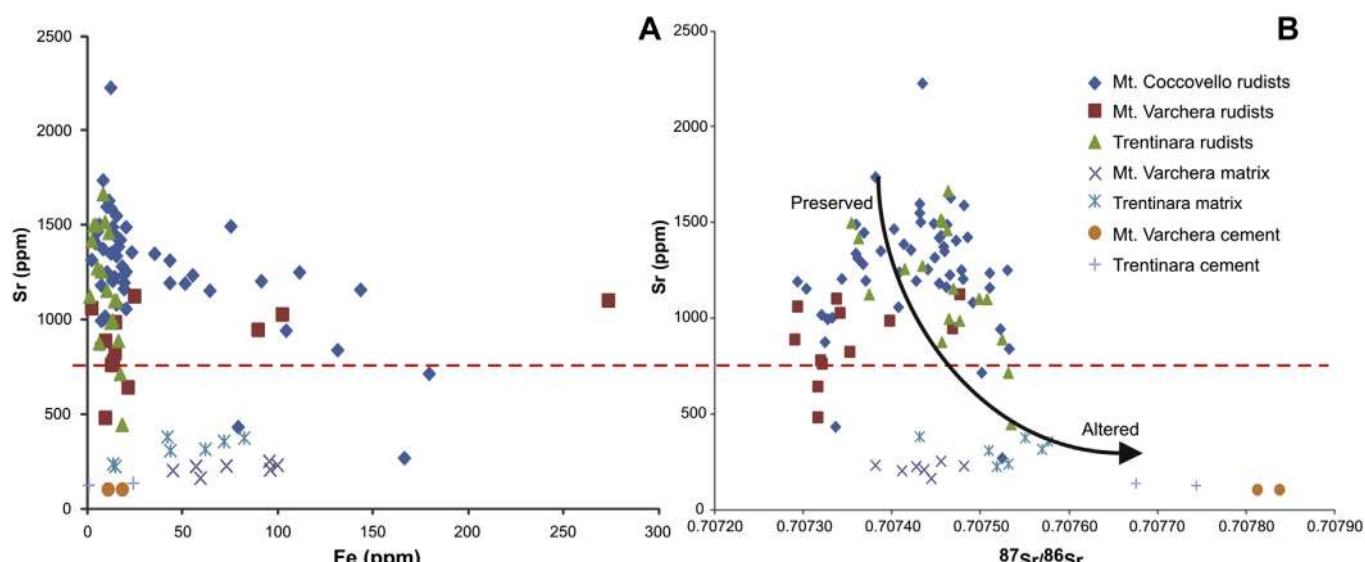


Fig. 11. Sr, Fe, concentration and $^{87}\text{Sr}/^{86}\text{Sr}$ in samples analysed for this study (A–B). The arrow indicates the diagenetic trend from pristine shells to altered shells to diagenetic calcite (micrite and cement). The dashed horizontal line indicates the threshold Sr concentration (750 ppm) used in this study. Above this value it is assumed that the original marine Sr-isotopic ratio has been retained (see text for further details). Note that most of the rudist samples analysed for this study have very low Fe concentrations and that late diagenetic cements, micritic matrix and poorly preserved rudist shells have lower Sr concentration and higher Sr-isotope values than pristine shells.

curve. The reference curve has two requisites: it is assumed to represent the record of the global ocean isotopic signal and is well calibrated to the geological time scale. When a good matching is found, the chemostratigraphic correlation with the well-dated reference section can be used to build an accurate age-model for the section under study. This empirical process of correlation by matching is often much more problematic for shallow-water carbonate successions, compared with hemipelagic and pelagic successions. Post-depositional diagenetic alteration (Dickson and Coleman, 1980; Allan and Matthews, 1982; Lohmann, 1988; Marshall, 1992), biological fractionation and local palaeoceanographic conditions may cause the carbon isotope signal of platform carbonates to deviate from the open ocean global signal (Weber and Woodhead, 1969; Patterson and Walter, 1994; see Immenhauser et al., 2008, for a recent review).

Strong covariation between $\delta^{13}\text{C}$ and $\delta^{18}\text{O}$ is commonly taken as proof of diagenetic alteration under the influx of meteoric water in the mixing zone (Allan and Matthews, 1982), or as a trend of progressively decreasing alteration within the freshwater phreatic zone (Swart, 2011). The isotope ratios cross-plot of fig. 12 shows no covariance between carbon and oxygen, indicating that neither of these processes left his mark on the samples selected from the studied sections. Strongly fluctuating, relatively low $\delta^{13}\text{C}$ values associated to an invariant $\delta^{18}\text{O}$ trend have been linked to meteoric diagenesis below subaerial exposure surfaces (Allan and Matthews, 1982; Lohmann, 1988). This pattern is observed in some segments of our isotopic profiles, accompanied by sedimentologic evidence of subaerial exposure (see Figs. 4, 5, 6). We did not attempt correlation by carbon isotope stratigraphy over these segments, considering that their original isotopic signal had been strongly overprinted by meteoric diagenesis.

The major features of the $\delta^{13}\text{C}$ curves of the studied sections, i.e. the lower frequency isotopic trends and excursions, are not associated to any specific lithofacies and persist across major facies changes. Therefore, we conclude that, while the higher order fluctuations could be the result of variations of environmental conditions on the platform, the low-frequency trends and the major excursions, and especially the positive ones, record the

long-term carbon isotope signal of the open ocean. A similar general conclusion was reached by Colombie et al. (2011) after a thorough evaluation of the carbon isotope records of Kimmeridgian shallow-marine carbonates of the Swiss Jura.

A correlation between the major features of the carbon isotope profiles recovered from the studied sections and the Late Cretaceous $\delta^{13}\text{C}$ carbonate reference curve of Jarvis et al. (2006) is shown in Fig. 13. The reference curve contains a very prominent positive excursion of about 3‰ in the Cenomanian-Turonian boundary (CTB) interval, corresponding with the oceanic anoxic event 2 (OAE2, Bonarelli event). Another sharp positive excursion, of about 1‰, marks the Turonian-Coniacian boundary. The reference curve contains many other lower amplitude events (<0.5‰). We agree with Föllmi and Godet (2013) that the signal to noise ratio in carbonate platform carbon isotope curves is usually too small for reliable identification of such minor events. Matching of the carbon isotope curves of the studied sections with the reference curve was constrained by independent tie-points, derived from biostratigraphy and SIS. The very prominent $\delta^{13}\text{C}$ positive excursion occurring near the base of the Mt. Coccovello and Mt. Varchera sections has been already correlated with the CTB event (Parente et al., 2007, 2008; Frijia and Parente, 2008b). Above the CTB, both the $\delta^{13}\text{C}$ curves show an interval of negative carbon isotope values which is likely the results of meteoric diagenesis. This is supported by the presence, in the corresponding segments of the studied sections, of subaerial exposure surfaces associated with microkarstic features and dolomitized breccias. This interval of negative $\delta^{13}\text{C}$ values is followed, both at Mt. Coccovello and at Mt. Varchera, by a positive excursion of about 2‰. We tentatively correlate this peak with the “Pewsey” event, which occurs in the uppermost part of the middle Turonian (Jarvis et al., 2006). This is a very minor event in the reference curve (<0.5‰) but it could have been amplified by local processes in shallow-water environments (Föllmi and Godet, 2013). Moreover, the correlation is strongly supported by SIS ages (Fig. 13). The successive $\delta^{13}\text{C}$ event that we used for correlation is the well pronounced positive peak found at 170 m from the base of the Mt. Coccovello section and at about 160 m from the base at Mt. Varchera. We correlate this peak to the latest Turonian “Hitch Wood”

Table 2
Strontium Isotope Stratigraphy of the studied sections.

Sample	Component	Section	Metres from the base	$^{87}\text{Sr}/^{86}\text{Sr}$	2 s.e. ($\times 10^{-6}$)	$^{87}\text{Sr}/^{86}\text{Sr}$ mean	2 s.e. mean ($\times 10^{-6}$)	Age (Ma)		
								Min	Preferred	Max
P 805C	Rudist	Trentinara	32.5	0.707374	7					
P 808 A	Rudist	Trentinara	33.5	0.707362	7					
P 808 C	Rudist	Trentinara		0.707354	7					
mean						0.707363	12	87.34	87.82	88.50
P 899 D	Rudist	Trentinara	114	0.707434	7					
P 899G	Rudist	Trentinara		0.707414	7					
mean						0.707424	20	83.71	85.98	86.50
P 941 A	Rudist	Trentinara	151	0.707463	7					
P 941 C	Rudist	Trentinara		0.707455	7					
mean						0.707459	8	82.40	83.12	84.20
P 966X	Rudist	Trentinara	178	0.707469	7					
P 966 B	Rudist	Trentinara		0.707462	6					
P 968C	Rudist	Trentinara	180	0.707476	7					
P 971A	Rudist	Trentinara	182.5	0.707464	7					
mean						0.707468	6	82.02	82.64	83.26
P1008A	Rudist	Trentinara	215.5	0.707507	7					
P1008D	Rudist	Trentinara		0.7074979598	7					
mean						0.707502	9	79.37	80.64	81.49
P323 A1a	Undet. bivalve	Mt. Coccovello	82.9	0.707361	7					
P323 A3a	Undet. bivalve	Mt. Coccovello	82.9	0.707363	6					
P325 A2a	Undet. bivalve	Mt. Coccovello	85.5	0.707363	7					
mean						0.707362	14	92.7	93.44	94.45
P 363 A	Rudist	Mt. Coccovello		0.707303	7					
P 363 B	Rudist	Mt. Coccovello	129.3	0.707293	7					
mean						0.707298	10	89.28	90.66	91.41
P401 A	Rudist	Mt. Coccovello		0.707332	7					
P401 B	Rudist	Mt. Coccovello	190.3	0.707324	7					
P404 A	Rudist	Mt. Coccovello		0.707320	7					
P404 B	Rudist	Mt. Coccovello	195.3	0.707327	7					
mean						0.707326	5	88.83	89.04	89.23
P423A	Rudist	Mt. Coccovello		0.707359	7					
P423B	Rudist	Mt. Coccovello	220.8	0.707367	7					
P425A	Rudist	Mt. Coccovello		0.707359	7					
P425B	Rudist	Mt. Coccovello		0.707361	7					
P425C	Rudist	Mt. Coccovello	224.3	0.707343	7					
mean						0.707358	3	87.72	88.08	88.36
P442A	Rudist	Mt. Coccovello		0.707370	7					
P442B	Rudist	Mt. Coccovello	255	0.707368	7					
mean						0.707369	17	87.06	87.63	88.47
P474AA	Rudist	Mt. Coccovello		0.707381	7					
P474AB	Rudist	Mt. Coccovello		0.707387	7					
P474AC	Rudist	Mt. Coccovello	278.3	0.707402	7					
mean						0.707390	12	86.59	87.08	87.56
P495AA	Rudist	Mt. Coccovello		0.707408	7					
P495AB	Rudist	Mt. Coccovello		0.707407	7					
P495AC	Rudist	Mt. Coccovello	302.3	0.707413	7					
mean						0.707409	14	85.80	86.51	87.07
P513A	Rudist	Mt. Coccovello		0.707427	7					
P513C	Rudist	Mt. Coccovello	317.8	0.707431	6					
P520A	Rudist	Mt. Coccovello		0.707434	7					
P520B	Rudist	Mt. Coccovello		0.707421	7					
P520C	Rudist	Mt. Coccovello	323.8	0.707440	7					
P525A	Rudist	Mt. Coccovello		0.707431	7					
P525B	Rudist	Mt. Coccovello	328.3	0.707432	7					
mean						0.707431	4	84.85	85.65	86.06
P568A	Rudist	Mt. Coccovello		0.707461	7					
P568B	Rudist	Mt. Coccovello	369.8	0.707447	7					
P570A	Rudist	Mt. Coccovello		0.707453	7					
P570B	Rudist	Mt. Coccovello	371.8	0.707448	7					
P572A	Rudist	Mt. Coccovello		0.707485	7					
P572B	Rudist	Mt. Coccovello	373.8	0.707455	7					
P574A	Rudist	Mt. Coccovello		0.707453	7					
P574B	Rudist	Mt. Coccovello	376	0.707459	7					
mean						0.707458	9	82.40	83.18	84.43
P581A	Rudist	Mt. Coccovello		0.707481	6					
P581B	Rudist	Mt. Coccovello	381.3	0.707466	7					
P582A	Rudist	Mt. Coccovello		0.707465	7					
mean						0.707471	10	81.65	82.48	83.33
P605A	Rudist	Mt. Coccovello		0.707478	7					
P605B	Rudist	Mt. Coccovello	412.3	0.707472	7					
mean						0.707475	17	81.00	82.26	83.55

(continued on next page)

Table 2 (continued)

Sample	Component	Section	Metres from the base	$^{87}\text{Sr}/^{86}\text{Sr}$	2 s.e. ($\times 10^{-6}$)	$^{87}\text{Sr}/^{86}\text{Sr}$ mean	2 s.e. mean ($\times 10^{-6}$)	Age (Ma)		
								Min	Preferred	Max
P614A	Rudist	Mt. Coccovello	422	0.707480	7	0.707480	24	79.89	81.97	83.71
P633C	Rudist	Mt. Coccovello	446.5	0.707510	7	0.707510	24	78.14	79.90	81.91
GF72 B	Rudist	Mt. Varchera		0.707290	6					
GF72 A	Rudist	Mt. Varchera	72.5	0.707293	7					
mean						0.707292	17	89.26	90.43	91.46
GF140	Rudist	Mt. Varchera	156.4	0.707323	7					
GF142 A	Rudist	Mt. Varchera	159.5	0.707319	7					
GF144	Rudist	Mt. Varchera	161	0.707322	7					
mean						0.707321	14	88.74	89.13	89.49
GF150 B	Rudist	Mt. Varchera		0.707341	7					
GF150 A	Rudist	Mt. Varchera		0.707337	7					
GF150	Rudist	Mt. Varchera	179.5	0.707336	7					
mean						0.707338	14	88.21	88.76	89.17
GF179	Rudist	Mt. Varchera	219.8	0.707397	7	0.707397	24	85.89	86.88	87.7

Numerical ages from McArthur et al. (2001; look-up table version 4: 08/04). Chronostratigraphy from Gradstein et al. (2004). See the text for details on the calculations of numerical ages and on the estimates of the precision.

event of Jarvis et al. (2006). SIS numerical ages of about 89 Ma, derived from levels bracketing this peak in both the sections, strongly support this correlation (Fig. 13). Above this event, the chemostratigraphic correlation becomes more problematic. Some segments can be convincingly correlated between the three carbonate platform sections but their correlation to the reference curve is less compelling (Fig. 13). We tentatively identified the “Santonian-Campanian Boundary Event” of Jarvis et al. (2006) in the Trentinara $\delta^{13}\text{C}$ curve by matching it with the positive peak at 170 m from the base of the section. Above this level, carbon isotope values show a marked negative trend, which could be the equivalent of the regular decrease of $\delta^{13}\text{C}$ values shown by the reference curve between the “Santonian-Campanian Boundary Event” and the mid-Campanian event of Jarvis et al. (2002, 2006). Correlation is even less compelling for the Mt. Coccovello section, where, based on SIS, the decrease of $\delta^{13}\text{C}$ values starts much earlier than the Santonian-Campanian boundary (Fig. 13).

5.2. Chronostratigraphic calibration of the Apennine carbonate platform biostratigraphy

After the first synthesis by Sartoni and Crescenti (1962), the two most widely used biostratigraphic schemes for the Mesozoic shallow-water carbonates of the central-southern Apennines have been proposed by Chiocchini and Mancinelli (1977) and by De Castro (1991). Chiocchini et al. (1994, 2008) revised the previous biozonation of Chiocchini and Mancinelli (1977). These biozonal schemes are very similar, with minor differences in the choice of the index species of the biozones and in the chronostratigraphic ages of the biozones. To this regards, it is worth stressing again that both Chiocchini et al. (1994, 2008) and De Castro (1991) state clearly that the chronostratigraphic ages of their biozones are only a crude approximations and are not substantiated by any direct correlation with the standard ammonite biozones, which are the foundation of Cretaceous chronostratigraphy.

In this study we have derived a chronostratigraphic age-model for the studied sections by integrating SIS and C-isotope stratigraphy (Fig. 14). This age model can be used to calibrate the chronostratigraphic age of the biostratigraphic events. This chemostratigraphically constrained chronostratigraphic calibration is relevant also for other central Tethyan carbonate platforms (i.e. the Apulian, Adriatic and Gavrovo-Tripolitza carbonate platforms) whose biostratigraphy is largely based on the same species of larger foraminifers which are used in the ACP. Also for these platforms the chronostratigraphic age of the biozones was so far poorly

constrained. The only chronostratigraphically reliable data have been recently produced for the Upper Cretaceous carbonates of the island of Brac (Adriatic platform) integrating SIS and biostratigraphy (Steuber et al., 2005).

The chart of the most important biostratigraphic events which have been recognised in the studied sections and their chronostratigraphic calibration is given in Fig. 15. It is worth mentioning that the ranges of many of the species appearing after the CTB extinction (Parente et al., 2008) extend until the top of the studied sections, which corresponds to the lower-middle Campanian according to our chemostratigraphic scheme. In other areas, these species are reported to range into the upper Campanian and Maastrichtian (Fleury, 1980; Steuber et al., 2005; Velic, 2007). For these species we can only constrain the age of the FO and give a minimum estimate of their LO.

The chronostratigraphic ranges of the most significant late Cenomanian taxa (*Cisalveolina fraasi*, *Chrysalidina gradata*, *Pseudodolitonella reicheli*, *Pseudorhapydionina dubia*, *Pseudorhapydionina casertana*, *Coxites zubairensis*, *Biconcava bentori*, *Vidalina radoicicae*) is mainly constrained by C-isotope stratigraphy (Parente et al., 2008; this study). According to the critical review by De Castro (1983), the total range of *C. fraasi* is limited to the upper Cenomanian. Fleury (1980) considered the range of this important marker reaching the lower Turonian whereas a late Cenomanian age is accepted in the recent schemes by Velic (2007) and Chiocchini et al. (2008). In the studied sections, the FO of *C. fraasi* is found at a level that can be correlated by carbon isotope stratigraphy to the middle part of the *Metoicoceras geslinianum* ammonite zone (Parente et al., 2007; this study). The LO is still within the same ammonite zone, at a level that can be correlated with the top of the *Rotalipora cushmani* planktic foraminiferal zone (Parente et al., 2008). In the ACP, most of the late Cenomanian larger foraminifers disappear together with *C. fraasi*. The only survivors are *C. gradata*, *P. reicheli* and *P. dubia*, which disappear 15–20 m above, in levels which can be correlated by carbon isotope stratigraphy with the lower part of the *Neocardioceras juddi* ammonite zone (i.e. in the latest Cenomanian) (Fig. 15). This two-steps pattern of larger foraminifers extinction during the latest Cenomanian has been related to the palaeoenvironmental perturbations accompanying the OAE2 (Parente et al., 2008). The low-diversity benthic foraminiferal assemblages of the uppermost Cenomanian-lower Turonian are characterized by few specimens belonging to small and architecturally simple morphotypes. These taxa, so far never described in detail, have recently been investigated making them useful for

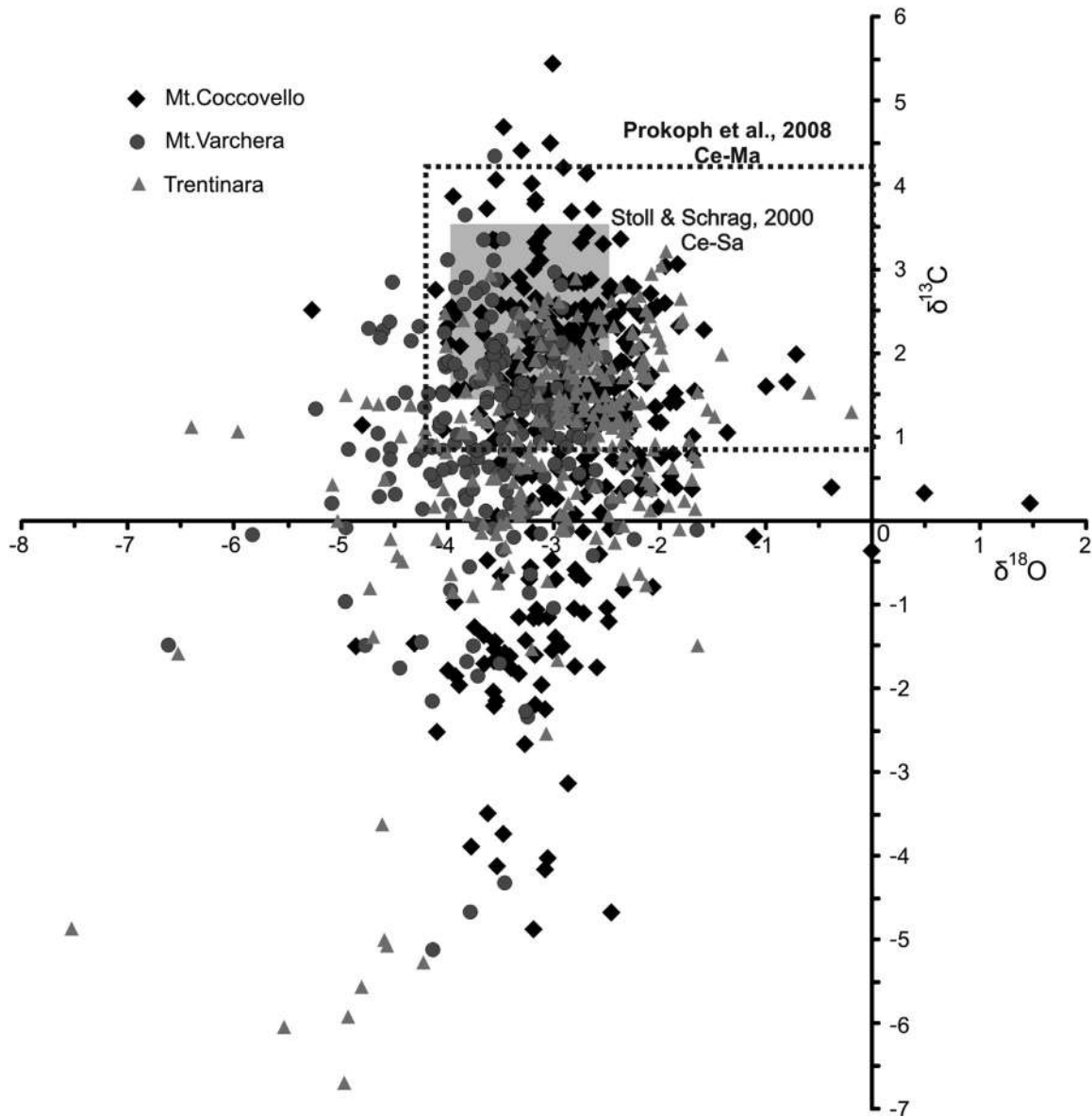


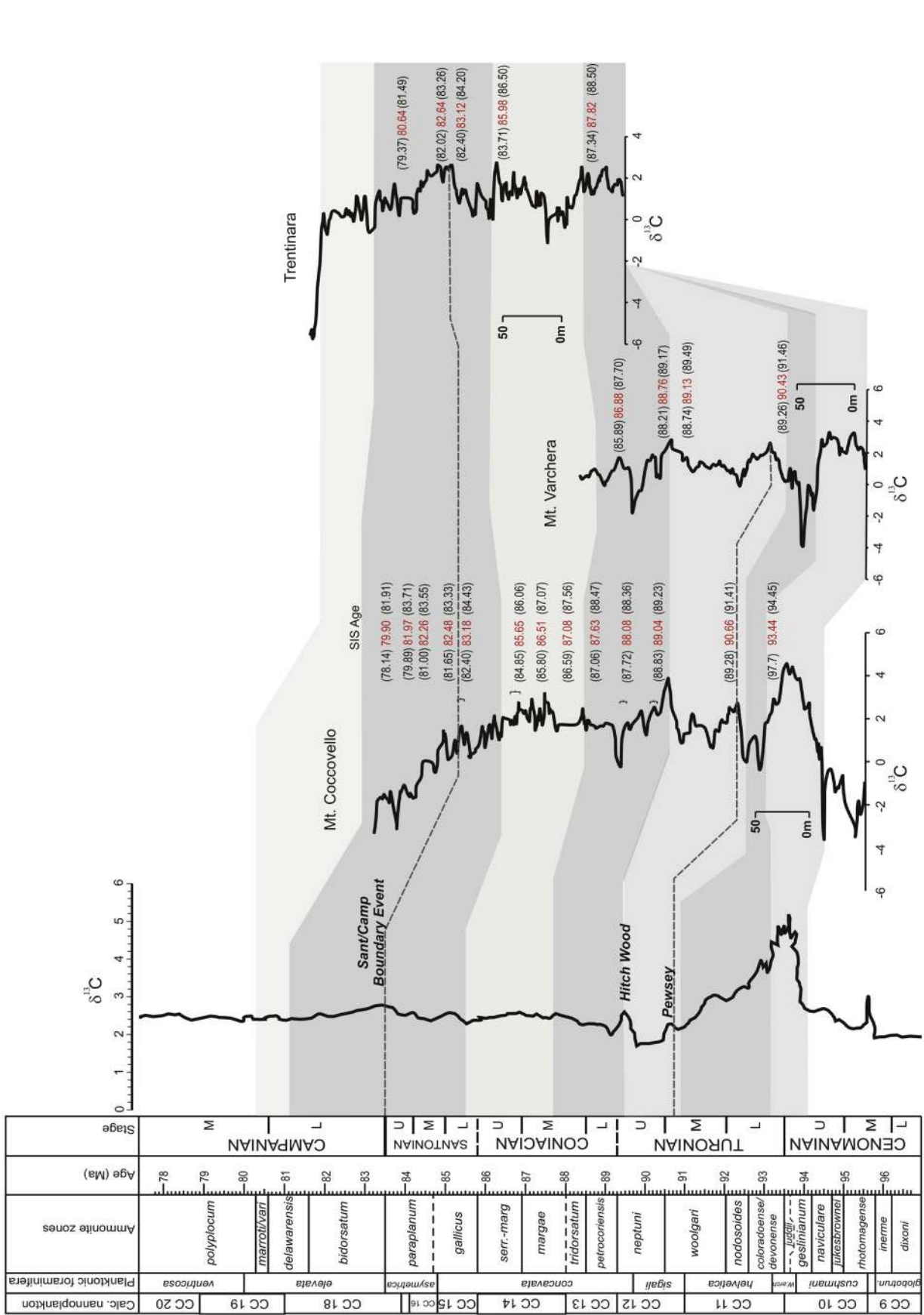
Fig. 12. Cross-plot of $\delta^{13}\text{C}$ vs. $\delta^{18}\text{O}$ for the three studied sections. The dataset shows no covariance between O and C isotopic values. Relatively depleted $\delta^{13}\text{C}$ values associated to an invariant $\delta^{18}\text{O}$ trend are probably due to the overprint of meteoric diagenesis (see text for further details). The shaded rectangle in the diagram indicates the isotopic field of Late Cretaceous pelagic carbonates of central Italy (Scaglia Fm; after Stoll and Schrag, 2000) whereas the dotted rectangle represents the range of well-preserved biotic calcite of shallow marine tropical-subtropical carbonates (after Prokoph et al., 2008).

future biostratigraphic use (Arriaga et al., submitted). One of the most commonly reported species was formerly cited as *Valvulamina picardi* (Chiocchini and Mancinelli, 1977) and has been later referred to *Nezzazatinella* cf. *aegyptiaca* (Chiocchini et al., 1994, 2008). According to our chemostratigraphic correlation, this species, that we indicate as *Nezzazatinella* sp., (following Arriaga et al., submitted for publication) appears in the uppermost Cenomanian, very close to the CTB (Figs. 14 and 15).

The first true Turonian newcomers are *Moncharmontia apenninica* and *Pseudocyclammia sphaeroidea*. These two taxa occur at the same level at Mt. Coccovello whereas *M. apenninica* FO is a few metres below *P. sphaeroidea* at Mt. Varchera (Fig. 14). Both these taxa were generally indicated as first occurring in the Turonian by De Castro (1991). According to Chiocchini et al. (2008), the FO of *M. apenninica* in the central Apennines is in the upper Turonian, while *P. sphaeroidea* appears considerably later, in the lower Coniacian. According to Velic (2007), both these species have their FO

in the upper Turonian, with *P. sphaeroidea* slightly preceding *M. apenninica*. According to our scheme the FO of these taxa is in the lowermost Turonian, at a level that can be correlated chemostratigraphically to the lower part of the Tethyan ammonite zone *Watinoceras devonense*.

Reticulinella kaeveri is present at Mt. Coccovello and Mt. Varchera in a very thin interval of about 10–12 m (Fig. 14). SIS data by Frijia and Parente (2008a) were compatible with two alternative options for the chronostratigraphic range of this species: the upper part of the middle Turonian or the upper part of the upper Turonian (see figure 6 in Frijia and Parente, 2008a). The integration of C-isotope stratigraphy with SIS indicates that the first alternative is the correct one: the range of *R. kaeveri* can be correlated with the upper part of the *Collignoceras woolgari* ammonite zone, in the upper part of the middle Turonian (Fig. 15). A slightly younger range (lower part of the upper Turonian) is reported by Chiocchini et al. (2008) in the central Apennines.



English Chalk carbon isotope reference curve (Jarvis et al., 2006)

Fig. 13. C-isotope correlation of the three studied sections of the Apennine Carbonate Platform with the Late Cretaceous C-isotope reference curve (Jarvis et al., 2006). Red numbers next to the isotope curves indicate the preferred SIS age whereas black numbers refer to the upper and lower age boundary (see text for further explanation). In the upper Cenomanian-Turonian interval there is a good match between the $\delta^{13}C$ curves of the studied sections and the reference curve. In the Coniacian-Campanian interval the correlation is more problematic but is well supported by Sr-isotope stratigraphy. Time scale from Gradstein et al. (2004). (For interpretation of the references to colour in this figure legend, the reader is referred to the web version of this article.)

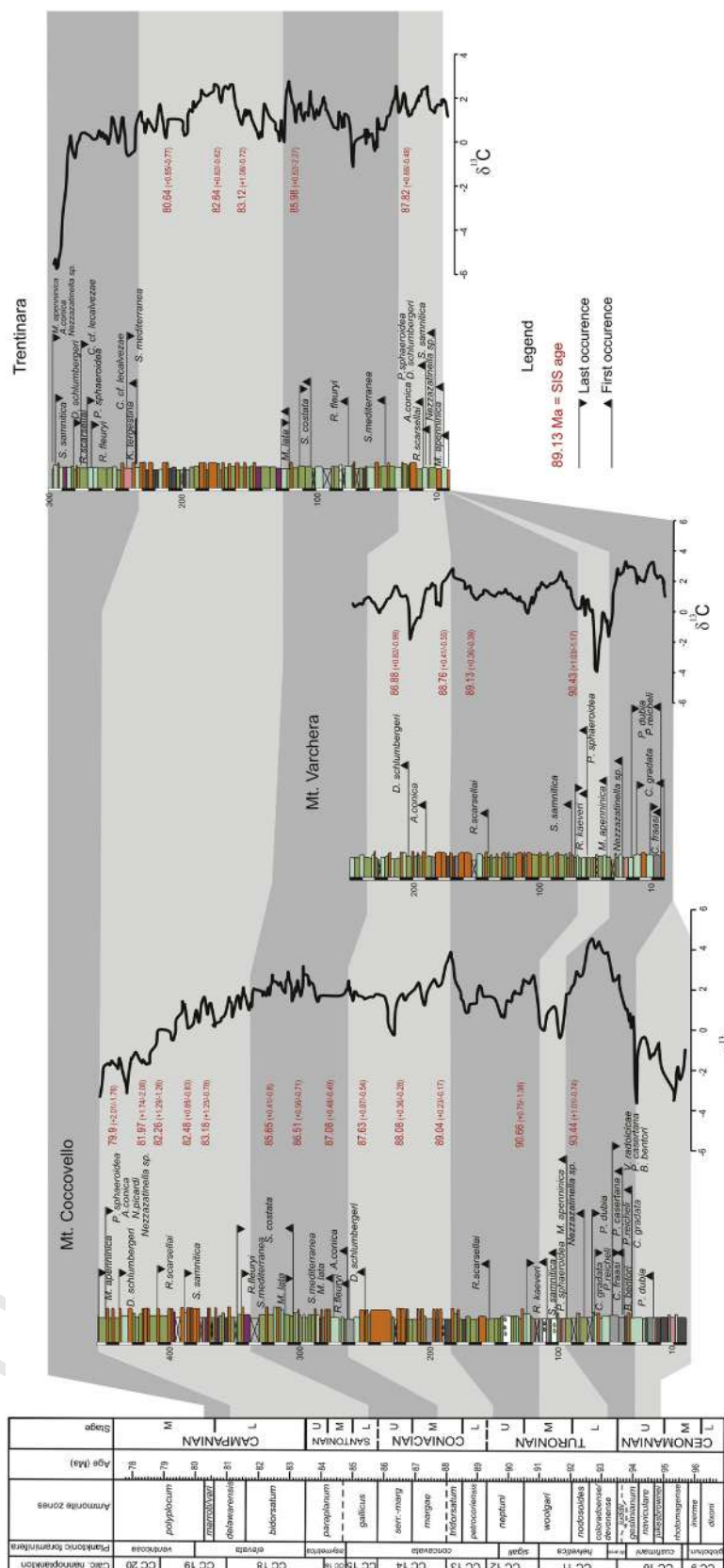


Fig. 14. Bio-chemostratigraphy of the Apennine Carbonate Platform. The chronostratigraphic calibration of the bioevents is constrained by C- and Sr-isotope stratigraphy. For key to colours refer to fig. 4. Time scale from Gradstein et al. (2004).

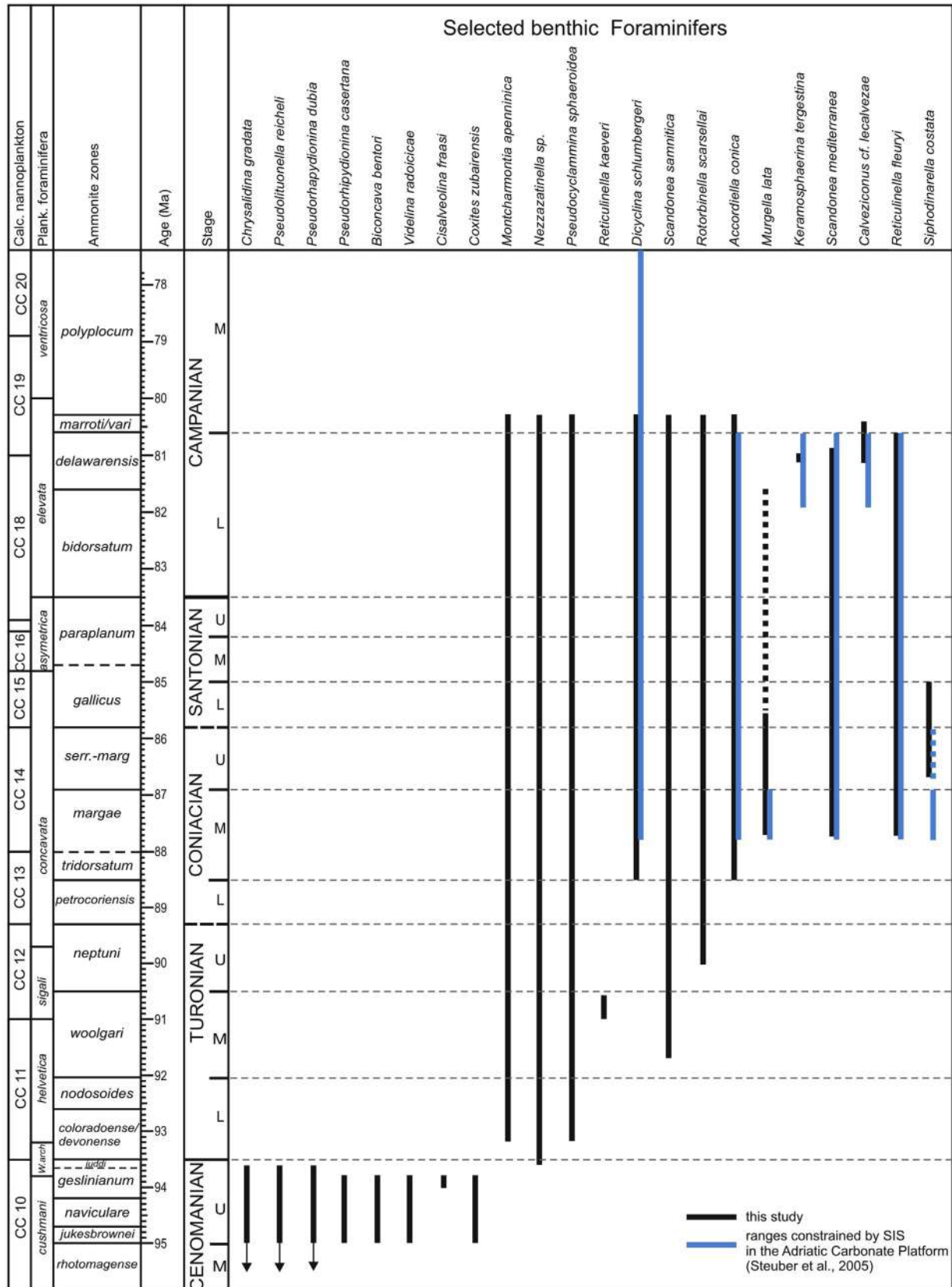


Fig. 15. Chronostratigraphic ranges of selected benthic foraminifers of the Apennine Carbonate Platform, based on the chemostratigraphic correlation of figures 13 and 14. The ranges of some species are truncated at the top by the unconformity capping the Upper Cretaceous rudist limestones. For some species there is a good match with the chronostratigraphic ranges obtained by Steuber et al. (2005) in the Adriatic Carbonate Platform. Notice that, for sake of comparison, the SIS ages of Steuber et al. (2005) have been recalculated with the look-up table of McArthur et al. (2001, version 4: 08/04), Time scale from Gradstein et al., 2004.

The FO of *Scandonea samnitica* can be precisely correlated with the lower part of the *Collignoceras woolgari* ammonite zones, which corresponds to the lower part of the middle Turonian (Fig. 14). The range of this species extends to the top of the studied sections (lower-middle Campanian). In the central Apennines a lower Coniacian-upper Santonian range is reported for this species by Chiocchini et al. (2008). According to Velic (2007) in the Adriatic Platform *S. samnitica* is present from the Coniacian to the upper Campanian. However, in the island of Brač this species has been reported from the lower part of the Gornji Humac fm., dated as early-middle Turonian by strontium and carbon isotope stratigraphy (Steuber et al., 2005; Korbar et al., 2012) (Fig. 15).

Rotorbinella scarsellai first occurs both at Mt. Coccovello and Mt. Varchera about 20m below the prominent positive C-isotope peak of the late Turonian (Fig. 14), at a level which can be very accurately correlated by SIS to the middle part of *Subprionocyclus neptuni* ammonite zone (Fig. 15). This age is slightly older than the base of the Coniacian reported as FO for the taxa by Chiocchini et al. (2008) in the central Apennines. On the other hand, a considerably younger FO (middle-upper Santonian) is reported by Velic (2007) in the Adriatic Platform.

Reticulinella fleuryi is first found both in the Mt. Coccovello and in the Trentinara section in levels which can be precisely dated by SIS as middle Coniacian and can be correlated to the middle part of the *Gauthiericeras margae* ammonite zone (Fig. 14). The range of this species extends to the top of the studied sections. *R. fleuryi* has been first described from the Upper Cretaceous deposits of the island of Brač (Croatia) by Cvetko et al. (1997). These authors found the species in the highest part of the Gornji Humac formation and in the Pučišća formation, and gave an upper Santonian-middle Campanian range. The same range is reported by Velic (2007) in the Adriatic Platform. However, SIS data on the Upper Cretaceous of the island of Brač support a middle Coniacian age for the upper part of the Gornji Humac Formation (Steuber et al., 2005). Furthermore, Schlagintweit and Sander (2008) found *R. fleuryi* at Weisswasser, in the Gousau Group of the Northern Alps of Austria, just beneath a rudist limestone which was dated by Sr-isotopes (Steuber, 2001) as middle Coniacian. These two isotopic ages agree with the middle Coniacian FO of *R. fleuryi* observed in the southern Apennines (Fig. 15).

The FO of *Accordiella conica* is at the lower-middle Coniacian boundary and can be correlated with the base of the *Peroniceras tridorsatum* ammonite biozone (Fig. 14). According to De Castro (1991) and Chiocchini et al. (2008) the range of *A. conica* is Coniacian-Campanian. The same range is indicated by Velic (2007) for the Adriatic Platform, but an FO in the lower-middle Coniacian is supported by SIS in the island of Brač (Steuber et al., 2005) (Fig. 15).

Dicyclina schlumbergeri first occurs few metres above the FO of *A. conica* at Mt. Varchera, while it is first found below the FO of *A. conica* at Mt. Coccovello (Fig. 14). Therefore this biostratigraphic event can be also referred to the base of the middle Coniacian. The range of this species extends to the top of the studied sections (lowermost middle Campanian). According to Cherchi and Schroeder (1990) the range of *D. schlumbergeri* is Coniacian-Santonian while Velic (2007) gives a Coniacian-Maastrichtian range. In the Upper Cretaceous of the island of Brač the FO of *D. schlumbergeri* is reported in the upper part of the Gornji Humac Fm., at a level that is dated as middle Coniacian by SIS (Steuber et al., 2005) (Fig. 15). It is worth noting that the determination of *Dicyclina* at the species level is problematic when centred sections through the embryonal apparatus are not available. Incorrect specific attribution could be the reason of the different stratigraphic ranges given for *D. schlumbergeri* by different authors.

Murgella lata has a narrow stratigraphic range in the studied sections. The FO of this taxa is in the middle Coniacian

(*Gauthiericeras margae* ammonite zone) whereas its LO is some 40 m above and can be dated as lowermost Santonian, close to the Coniacian-Santonian boundary (Fig. 14). A late Coniacian-Santonian age is reported for this species in the Apulian platform (Luperto-Sinni and Ricchetti, 1978) whereas Velic (2007) reported a Santonian-lower Campanian range in the Adriatic Platform. The middle Coniacian age for the FO of *M. lata* is supported by SIS also in the Upper Cretaceous limestones of the island of Brač (Steuber et al., 2005) (Fig. 15). Recent investigations in the central Apennines (L. Consorti, personal communication) reported the occurrence of *M. lata* some 10 m below the FO of *K. tergestina*. This would support a wider range, extending into the lower Campanian (see below).

Scandonea mediterranea first occurs together with *M. lata* in the middle Coniacian and disappears ~55 m below the top of Trentinara section, in a level which can be dated as early Campanian by SIS and correlated with the *Menabites (Delawarella) delawarensis* ammonite zone (Fig. 14). Velic (2007) reported the range of this taxa as base Santonian-upper Campanian, whereas Chiocchini et al. (2008) give an upper Santonian-lower Campanian range. Finally, Steuber et al. (2005) reported a Coniacian-lower Campanian range, constrained by SIS (Fig. 15).

Siphodinarella costata is a benthic foraminifer recently described by Schlagintweit et al. (2014) from shallow-water carbonate deposits of the Adriatic Carbonate platform (Croatia and Slovenia). In Croatia it occurs in the upper part of the Gornji Humac Fm, in association with *M. lata* in an interval which would correspond to the middle-?upper Coniacian using the SIS dating of Steuber et al. (2005) (Fig. 15). However, Schlagintweit et al. (2014) state that its stratigraphic range could be even wider. In the Apennine platform *S. costata* occurs in a narrow interval both at Mt. Coccovello and Trentinara (~40 and 10 m respectively) overlapping with the upper part of the range of *M. lata* (Fig. 14). Chronostratigraphic calibration by carbon isotopes and SIS indicates that the range of this species in the ACP is upper Coniacian-lower Santonian.

Keramosphaerina tergestina occurs at Trentinara only in two beds at about 235 m from the base of the section (Fig. 14). Combining carbon isotope stratigraphy and SIS we correlate this level with the *Menabites (Delawarella) delawarensis* ammonite zone, in the upper part of the lower Campanian. The occurrence of a dm-to m-thick marker level with *K. tergestina* is also reported from the upper part of the Aurisina Limestones in the Trieste Karst area (Caffau et al., 2000; Venturini, 2005). The age of this level is commonly considered as very close to the Santonian-Campanian boundary, with some support also from SIS (Cestari, 2002; Maritan et al., 2003; Venturini, 2005). Also in the central Apennines this species is reported to occur very close to the Santonian-Campanian boundary (Chiocchini et al., 2008). A Santonian-lower Campanian range is reported by Velic (2007) for *K. tergestina* in the Adriatic Platform, but the largest specimens are said to occur only in the uppermost Santonian-lowermost Campanian. SIS data from Steuber et al. (2005) supports a lower to middle Campanian range for both *K. tergestina* and the orbitolinid *Calveziconus cf. lcalvezae*, with an FO in the middle part of the lower Campanian (Fig. 15). Furthermore Sr-isotope values from levels yielding the FO of *K. tergestina* and *C. cf. lcalvezae* from Brač island are very close to the isotopic values obtained for levels about 15 m below the FO of these two taxa in southern Apennines ($0.707481 \pm 9 \cdot 10^{-6}$ vs $0.7007502 \pm 9 \cdot 10^{-6}$). In the Trentinara section *Calveziconus cf. lcalvezae* first occurs in the *K. tergestina* beds and is found up section for some more 35 m (Fig. 14). Its LO can be dated as earliest middle Campanian. A larger range, covering almost the whole Campanian, is reported for this species in the Adriatic Platform (Velic, 2007). However, it is important to note that Fleury (1980, see also Fig. 1) reported in the lower Campanian of Greece the presence

of a taxon, called Orbitolinides K, which occurs immediately above the LO of *K. tergestina*. Unfortunately, Fleury (1980) does not give any photograph of this taxon and therefore a direct comparison with the southern Apennine specimens is not possible.

5.3. Upper Cretaceous biostratigraphy of the Apennine Carbonate Platform

The re-evaluation of the ranges of the main foraminiferal taxa of the Upper Cretaceous deposits of the Apennine platform allowed us to revise and improve the biozonation scheme currently adopted for the central and southern Apennines (Chiocchini et al., 2008; Fig. 1). Moreover, for the first time the larger foraminiferal biozones can be anchored to the chronostratigraphic scale by isotope stratigraphy (Fig. 16).

Chiocchini et al. (2008) reported three biozones covering the interval upper Cenomanian-lower Campanian:

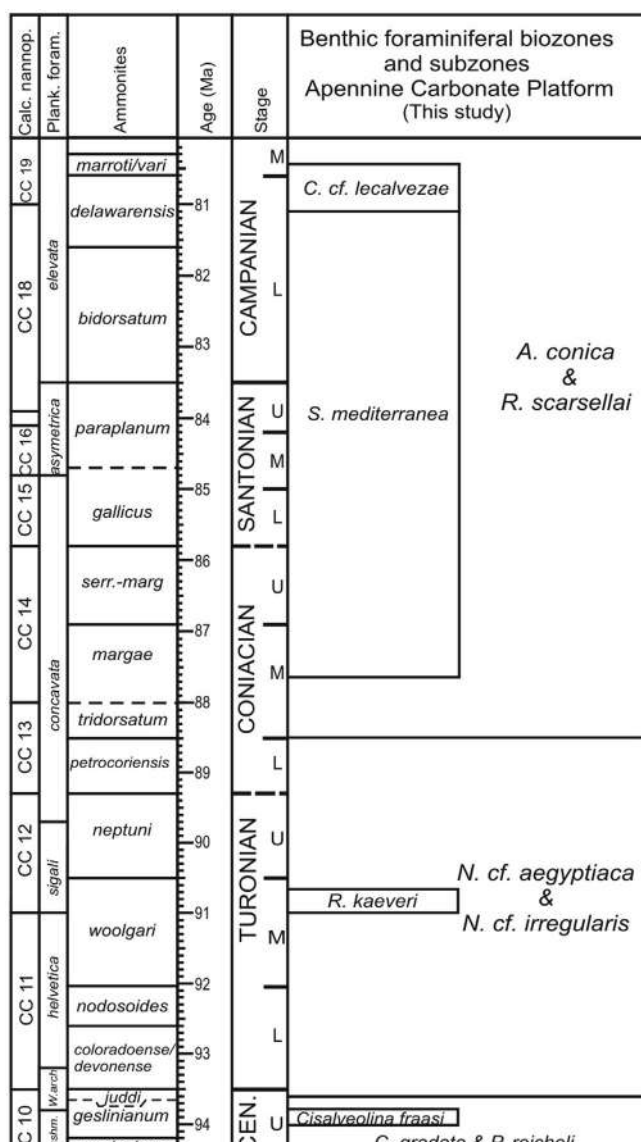


Fig. 16. Refined late Cenomanian-Maastrichtian biostratigraphy of the Apennine Carbonate Platform. The larger foraminiferal biozones of the Chiocchini et al. (2008) scheme have been anchored to the chronostratigraphic scale by isotope stratigraphy. Moreover, we propose four new subzones, which increase considerably the biostratigraphic resolution (see text for details).

Chrysalidina gradata and *Pseudolituonella reicheli* zone, defined at the base by the FO of *C. gradata* and at the top by the LO of these two taxa. According to Chiocchini et al. (2008) this biozone has a late Cenomanian age. Our data allow to precisely correlate the top of this biozone with the lower part of the *Neocardioceras juddi* ammonite zone in the uppermost Cenomanian (Fig. 16).

Nezzazinella. cf. aegyptiaca and *Nummuloculina cf. irregularis* zone. It extends from the LO of *C. gradata* and *P. reicheli* to the FO of *A. conica* and *R. scarsellai*. Chiocchini et al. (2008) reported a Turonian age for this biozone. Our data place the lower limit of the biozone in the uppermost Cenomanian and the upper limit at the lower/middle Coniacian boundary correlatable with the base of the *Peroniceras tridorsatum* ammonite zone (Fig. 16).

Accordiella conica and *Rotorbinella scarsellai* zone. It is defined at the base by the FO of *A. conica* and *R. scarsellai* and at the top by the LO of these two taxa. Chiocchini et al. (2008) give a Coniacian-Campanian age. Our chemostratigraphic data constrain the lower limit of this biozone at the lower/middle Coniacian boundary whereas its upper limit extends beyond the lower/middle Campanian boundary (Fig. 16).

Besides precisizing the chronostratigraphic age of the biozones of the Chiocchini et al. (2008) scheme, we propose to refine it by adding four subzones (Fig. 16):

Cisalveolina fraasi subzone, defined by the total stratigraphic range of *C. fraasi*. Its chronostratigraphic range is upper Cenomanian, corresponding to the middle part of the *Metoiceras geslinianum* ammonite zone.

Reticulinella kaeveri subzone, defined by the total stratigraphic range of *R. kaeveri*. Its chronostratigraphic range is in the upper part of the middle Turonian and can be precisely correlated with upper part of *Collignoceras woolgari* ammonite zone.

Scandonea mediterranea sub-zone, between the FO of *S. mediterranea* and the FO of *Calveziconus cf. lecalvezae*. The chronostratigraphic range of this subzone extends from the middle part of the middle Coniacian (middle part of *Gauthiericeras margae* ammonite zone) to the upper part of the lower Campanian (upper part of the *Menabites (Delawarella) delawarensis* ammonite zone). The biostratigraphic range of *S. mediterranea* extends for a few metres into the following subzone.

Calveziconus cf. lecalvezae subzone, defined by the total stratigraphic range of *C. lecalvezae*. Its chronostratigraphic range extends from the upper part of the lower Campanian (upper part of the *Menabites (Delawarella) delawarensis* ammonite zone) to the lowermost middle Campanian (lower part of *Hoplitoplaticeras marroti* ammonite zone).

6. Conclusions

The integration of carbon- and strontium isotope stratigraphy allowed us to establish a well constrained chronostratigraphic scheme for the Upper Cretaceous (upper Cenomanian-middle Campanian) shallow-water carbonates of the Apennine Carbonate Platform (southern Italy). The main advantage of using the two methods in conjunction is that Sr-isotope stratigraphy provides independent tie points that facilitate the correlation of the carbonate platform $\delta^{13}\text{C}$ curves with the reference curve of the English Chalk. Then, carbon isotope stratigraphy can be used to further enhance stratigraphic resolution.

The age model established by isotope stratigraphy allowed us to constrain for the first time the chronostratigraphic age of the main biostratigraphic events found in the Apennine Carbonate Platform (FOs and LOs of larger foraminifers) and to correlate them with the standard zones of ammonites, planktic foraminifers and calcareous nannoplankton. This result is of great interest because the same species are found in other peri-Tethyan carbonate platforms, from

the Adriatic Platform of Croatia, Serbia, Montenegro and Albania, to the Pre-Apulian Platform of the Ionian islands and the Gavrovo Platform of continental Greece, to the carbonate platforms of Turkey, the Levant Platform of Sinai and Israel and the carbonate platforms of the Arabian Plate. For the few species for which the chronostratigraphic range has been already constrained elsewhere by isotope stratigraphy (i.e. Steuber et al., 2005; Korbar et al., 2012; for the Adriatic Platform), it can be shown that it is synchronous across different platforms. Future work could establish a well constrained larger foraminiferal biostratigraphic scheme for the peri-Tethyan Upper Cretaceous carbonate platforms, perfectly correlated with the standard ammonite zones. Moreover, strontium isotope stratigraphy can be used as the foundation of a standard larger foraminiferal biozonation across different facies (inner platform to platform margin) and different palaeobiogeographic provinces (from the Caribbean to the Pyrenean realm, to the northern and southern Tethyan margins).

The refined stratigraphy of the Upper Cretaceous shallow-water carbonates of the Apennine Carbonate Platform proposed in this paper open many interesting research avenues. Some of the most promising ones include:

- Refining the regional sea-level history and comparing it with reference sea-level curves (Miller et al., 2004; Haq, 2014; see also the discussion in Steuber and Schlüter, 2012) to better address the hypothesis of glacio-eustatic sea-level changes during the Late Cretaceous greenhouse (Bornemann et al., 2008; Galeotti et al., 2009; Parente et al., 2010; MacLeod et al., 2013).
- Looking at the evolution of the Upper Cretaceous rudist limestones of southern Italy in the framework of global palaeoclimatic and palaeoceanographic changes.
- Constraining the timing and addressing the causes of the final demise of the Apennine Carbonate Platform after more than 140 my of nearly continuous shallow-water carbonate sedimentation from the Late Triassic to the middle Campanian.

Acknowledgements

Laura Galluccio (Badley Ashton) and Azzurra D'Atri (Eni, E&P division) are greatly acknowledged for their support and help in the field. We are grateful to Prof. Esmeralda Caus (UAB) for helpful advice. Dr. Dieter Buhl (Ruhr-Universität, Bochum) is warmly thanked for taking care of the geochemical analyses. We are finally grateful to Christine Fisher (Potsdam University) for her help with samples preparation.

The editor of Cretaceous Research Eduardo Koutsoukos is greatly acknowledged for his useful suggestions and his help with the manuscript. We are grateful to Felix Schlagintweit and an anonymous reviewer for their careful review and comments which improved the manuscript. This paper has been partly funded by MIUR-PRIN 2010-11 (prot. 2010X3PP8J).

References

- Al-Aasm, I.S., Veizer, J., 1986. Diagenetic stabilization of aragonite and low-Mg calcite. I. Trace elements in rudists. *Journal of Sedimentary Petrology* 56, 763–770.
- Albrich, S., Frijia, G., Parente, M., Caus, E., 2014. The evolution of the earliest representative of the genus *Orbitoides*: Implication for Upper Cretaceous biostratigraphy. *Cretaceous Research* 51, 22–34.
- Allan, J.R., Matthews, R.K., 1982. Isotope signature associated with early meteoric diagenesis. *Sedimentology* 29, 797–809.
- Amodio, S., Ferreri, V., D'Argenio, B., Weissert, H., Sprovieri, M., 2008. Carbon-isotope stratigraphy and cyclostratigraphy of shallow-marine carbonates: the case of San Lorenzello, Lower Cretaceous of southern Italy. *Cretaceous Research* 29, 803–813.
- Arnaud, H., Arnaud-Vanneau, A., Blanc-Alétru, M.C., Adatte, T., Argot, M., Delanoy, G., Thieuloy, J.P., Vermeulen, J., Virgone, A., Virlovet, B., Wermeille, S.,

1998. Répartition stratigraphique des orbitolinidés de la plate-forme urgo-nienne subalpine et jurassienne (SE de la France). *Géologie Alpine* 74, 3–89.
- Arnaud, H., 2005. The South-East France Basin (SEFB) and its Mesozoic evolution. In: Adatte, T., Arnaud-Vanneau, A., Arnaud, H., Blanc-Alétru, M.-C., Bodin, S., Carriro-Schaffhauser, E., Föllmi, K.B., Godet, A., Raddadi, M.C., Vermeulen, J. (Eds.), *The Hauterivian-Lower Aptian Sequence Stratigraphy from Jura Platform to Vocontian Basin: a Multidisciplinary Approach*, *Géologie Alpine, Colloques et Excursions*, 7, pp. 5–28.
- Arriaga, M.E., Frijia, G., Parente, M., Caus, E., 2014. Benthic foraminifera in the aftermath of the Cenomanian-Turonian boundary extinction event in the carbonate platform facies of the southern Apennines (Italy). *Journal of Foraminiferal Research* (submitted for publication).
- Banner, J.L., 1995. Application of the trace element and isotope geochemistry of strontium to studies of carbonate diagenesis. *Sedimentology* 42, 805–824.
- Boix, C., Frijia, G., Vicedo, V., Bernaus, J.M., Di Lucia, M., Parente, M., Caus, E., 2011. Larger foraminiferal distribution and strontium isotope stratigraphy of the La Cova limestones (Coniacian – Santonian, Serra del Montsec, Pyrenees, NE Spain). *Cretaceous Research* 32, 806–822.
- Bonardi, G., D'Argenio, B., Perrone, V., 1988. Carta Geologica dell'Appennino meridionale. SELCA, Firenze.
- Bornemann, A., Norris, R.N., Friedrich, O., Beckmann, B., Schouten, S., Sinninghe Damsté, J.S., Vogel, J., Hofmann, P., Wagner, T., 2008. Isotopic Evidence for Glaciation during the Cretaceous Supergreenhouse. *Science* 319, 189–192.
- Bosellini, A., 2002. Dinosaurs “re-write” the geodynamics of the eastern Mediterranean and the paleogeography of the Apulia Platform. *Earth-Science Reviews* 59, 211–234.
- Brand, U., Veizer, J., 1980. Chemical diagenesis of a multicomponent carbonate system: 1. Trace elements. *Journal of Sedimentary Petrology* 50, 1219–1236.
- Brand, U., Jiang, G., Azmy, K., Bishop, J., Montanez, I.P., 2012. Diagenetic evaluation of a Pennsylvanian carbonate succession (Bird Spring Formation, Arrow Canyon, Nevada, U.S.A.) - 1: Brachiopod and whole rock comparison. *Chemical Geology* 308–309, 26–39.
- Brand, U., Logan, A., Bitner, M.A., Grieshaber, E., Azmy, K., Buhl, D., 2011. What is the ideal proxy of Paleozoic seawater chemistry? *Memoirs of the Association of Australasian Palaeontologists* 41, 9–24.
- Burla, S., Heimhofer, U., Hochuli, P.A., Weissert, H., Skelton, P., 2008. Changes in sedimentary patterns of coastal and deep sea successions from the North Atlantic (Portugal) linked to Early Cretaceous environmental change. *Palaeogeography, Palaeoclimatology, Palaeoecology* 257, 38–57.
- Caffau, M., Colizza, E., Melis, R., Pugliese, N., Tsakiridou, E., Andriani, F., 2000. Il Santoniano-Campaniano del corso triestino: l'orizzonte a *Keramosphærina tergestina* (Stache). *Studi Trentini di Scienze Naturali* 77, 73–79.
- Carannante, G., Graziano, R., Ruberti, D., Simone, L., 1997. Upper Cretaceous temperate-type open shelves from northern (Sardinia) and southern (Apennines-Apulia) Mesozoic Tethyan margins. In: James, N.P., Clarke, J.A.D. (Eds.), *Cool-water carbonates*, SEPM Special Publication, 56, pp. 309–325.
- Carannante, G., Ruberti, D., Sirna, G., 1998. Lower Senonian rudist limestones in the Sorrento Peninsula sequences (southern Italy). *Geobios* 22, 47–68.
- Carannante, G., Graziano, R., Pappone, G., Ruberti, D., Simone, L., 1999. Depositional system and response to sea-level oscillation of the Senonian foramol-shelves. Examples from central Mediterranean areas. *Facies* 40, 1–24.
- Carannante, G., Ruberti, D., Sirna, M., 2000. Upper Cretaceous ramp limestones from the Sorrento Peninsula (southern Apennines, Italy): micro- and macrofossil associations and their significance in the depositional sequences. *Sedimentary Geology* 132, 89–123.
- Carpenter, S.J., Lohmann, K.E., 1992. Sr/Mg ratios of modern marine calcite: empirical indicators of ocean chemistry and precipitation rate. *Geochimica Cosmochimica Acta* 56, 1837–1849.
- Caus, E., Bernaus, J.M., Gómez-Garrido, A., 1996. Biostratigraphic utility of the species of the genus *Orbitoides*. *Journal of Foraminiferal Research* 26, 124–136.
- Caus, E., Parente, M., Vicedo, V., Frijia, G., Martínez, R., 2013. *Broeckina gassoensis* sp. nov., a larger foraminiferal index fossil for the middle Coniacian shallow-water deposits of the Pyrenean Basin (NE Spain). *Cretaceous Research* 45, 76–90.
- Cestari, R., Pons, J.M., 2004. Coniacian-Santonian rudist facies in Cilento (southern Italy). *CFS Courier Forschungsinstitut Senckenberg* 247, 175–192.
- Cestari, R., 2002. Strontium isotope signature of the main Upper Cretaceous rudist events in the Periadriatic Domain. In: Vlahovic, I., Korbar, T. (Eds.), *Abstracts and Excursion Guidebook. Sixth Int. Congress on Rudists*, Rovinj, pp. 16–17. Zagabria.
- Channell, J.E.T., D'Argenio, B., Horvath, F., 1979. Adria, the African Promontory, in Mesozoic Mediterranean palaeogeography. *Earth-Science Reviews* 15, 213–292.
- Cherchi, A., Schroeder, R., 1990. *Keramosphærina sarda* n. sp. Larger foraminifera (Miliolacea) from the Coniacian of Sardinia. *C. R. Acad. Sci., S. II, Mec. Phys. Chim. Sc. de l'Univ. Sc. de la Terre* 310 (n. 11), 1567–1572.
- Chiocchini, M., Mancinelli, A., 1977. Microbiostratigrafia del Mesozoico in facies di piattaforma carbonatica dei Monti Aurunci (Lazio meridionale). *Studi Geologici Camerti* 3, 109–152.
- Chiocchini, M., Chiocchini, R.A., Didaskalou, P., Potetti, M., 2008. Microbiostratigrafia del Triassico superiore, Giurassico e Cretacico in facies di piattaforma carbonatica del Lazio centro-meridionale e Abruzzo: revisione finale. In: Chiocchini, M. (Ed.), *Memorie Descrittive della Carta Geologica d'Italia*, Torino, 84, pp. 5–170.
- Chiocchini, M., Farinacci, A., Mancinelli, A., Molinari, V., Potetti, M., 1994. Biostratigrafia a foraminiferi, diaciladali e calpionelle delle successioni carbonatiche mesozoiche dell'Appennino centrale (Italia). In: Mancinelli, A. (Ed.),

- Biostratigrafia dell'Italia centrale. Studi Geologici Camerti, Volume Speciale, pp. 9–129.
- Clavel, B., Busnardo, R., Charollais, J., Conrad, M., Granier, B., 2009. Nouvelles données sur la répartition biostratigraphique des orbitolinidés à l'Hauterivien supérieur, au Barrémien et à l'Aptien inférieur dans le Sud-Est de la France et le Jura franco-suisse. *Archives des Sciences* 62, 125–146.
- Clavel, B., Busnardo, R., Charollais, J., Conrad, M., Granier, P.B., 2010. Répartition biostratigraphique des orbitolinidés dans la biozonation à ammonites (plate-forme urgonienne du Sud-Est de la France) Partie 1: Hauterivien supérieure Barrémien basal. *Carnets de Géologie/Notebooks on Geology* 6, 1–53.
- Colombie, C., Lécuyer, C., Strasser, A., 2011. Carbon- and oxygen isotope records of palaeoenvironmental and carbonate production changes in shallow-marine carbonates (Kimmeridgian, Swiss Jura). *Geological Magazine* 148, 133–153.
- Cvetko, B., Gusić, I., Schroeder, R., 1997. *Reticulinella fleuryi* n.sp. (Foraminifera) from the Upper Cretaceous (Upper Santonian–Middle Campanian) of the Island of Brač, Croatia. *Revue de Micropaléontologie* 40, 131–139.
- D'Argenio, B., Alvarez, W., 1980. Stratigraphic evidence for crustal thickness changes on the southern Tethyan margin during the Alpine cycle. *GSA Bulletin* 91, 681–689.
- D'Argenio, B., Ferreri, V., Weissert, H., Amodio, S., Buonocunto, F.P., Wissler, L., 2004. A multidisciplinary approach to global correlation and geochronology: the Cretaceous shallow-water carbonates of southern Apennines, Italy. In: D'Argenio, B., Fischer, A.G., Premoli Silva, I., Weissert, H., Ferreri, V. (Eds.), *Cyclostratigraphy: Approaches and Case Histories*. SEPM Special Publication, 81, pp. 103–122.
- D'Argenio, B., Pescatore, T., Scandone, P., 1973. Schema geologico dell' Appennino meridionale (Campania e Lucania). *Quaderni Accademia Nazionale dei Lincei* 183, 383–396.
- Davey, S.D., Jenkyns, H.C., 1999. Carbon-isotope stratigraphy of shallow-water limestones and implications for the timing of Late Cretaceous sea-level rise and anoxic events (Cenomanian–Turonian) of the peri-Adriatic carbonate platform, Croatia. *Eclogae Geologicae Helveticae* 92, 163–170.
- De Castro, P., 1983. *Cisalveolina fraasi* (Gümbel) Reichel, Foraminifera: diffusione geografica e problem stratigrafici. *Bollettino Società dei Naturalisti in Napoli* 90, 99–130.
- De Castro, P., 1991. Mesozoic. In: Barattolo, F., De Castro, P., Parente, M. (Eds.), *Field Trip Guide-Book, 5th International Symposium on Fossil Algae*. Giannini editore, Napoli, pp. 21–38.
- DePaolo, D.J., Ingram, B.L., 1985. High resolution stratigraphy with strontium isotopes. *Science* 277, 938–941.
- Dercourt, J., Zonenshain, L.P., Ricou, L.E., Kazmin, V.G., Le Pichon, X., Knipper, A.L., Grandjacquet, C., Sbertshikov, I.M., Geyssant, J., Lepvrier, C., Pechersky, D.H., Boulou, J., Sibuet, J.-C., Savostin, L.A., Sorokhtin, O., Westphal, M., Bazhenov, M.L., Lauer, J.-P., Biju-Duval, B., 1986. Geological evolution of the Tethys belt from the Atlantic to the Pamirs since the Lias. *Tectonophysics* 123, 241–315.
- Di Lucia, M., Trecalli, A., Mutti, M., Parente, M., 2012. Bio-chemostratigraphy of the Barremian – Aptian shallow-water carbonates of the southern Apennines (Italy): pinpointing the OAE1a in a Tethyan carbonate platform. *Solid Earth* 3, 1–28.
- Di Stefano, R., Fiorentino, A., Marino, M., Perini, P., 2011. Verso uno schema litostatigrafico dell'Appennino meridionale. *Rendiconti online della Società Geologica Italiana* 12, 59–61.
- Dickson, J.A.D., Coleman, M.L., 1980. Changes in carbon and oxygen isotope composition during limestone diagenesis. *Sedimentology* 27, 107–118.
- Elrick, M., Molina-Garza, R., Duncan, R., Snow, L., 2008. C-isotope stratigraphy and palaeoenvironmental changes across OAE 2 (mid Cretaceous) from shallow-water platform carbonates of southern Mexico. *Earth Planetary Science Letters* 277, 295–306.
- Ferreri, V., Weissert, H., D'Argenio, B., Buonocunto, F.P., 1997. Carbon-isotope stratigraphy: a tool for basin to carbonate platform correlation. *Terra Nova* 9, 57–61.
- Fleury, J.J., 1980. L. Publ. Soc. Geol. Du Nord 4 es zones de Gavrovo–Tripolitza et du Pinde–Olnos (Grece continentale et Peloponèse du Nord). Evolution d'une plateforme et d'un bassin dans leur cadre alpin, pp. 1–651.
- Föllmi, K., Godet, A., 2013. Palaeoceanography of Lower Cretaceous Alpine platform carbonates. *Sedimentology* 60, 131–151.
- Frijia, G., Parente, M., 2008a. *Reticulinella kaeveri* Cherchi, Radoičić and Schroeder: a marker for the middle upper Turonian in the shallow-water carbonate facies of the peri-adriatic area. *Bollettino della Società Geologica Italiana* 127, 275–284.
- Frijia, G., Parente, M., 2008b. Strontium isotope stratigraphy in the upper Cenomanian shallow-water carbonates of the southern Apennines: short-term perturbations of marine $^{87}\text{Sr}/^{86}\text{Sr}$ during the oceanic anoxic event 2. *Palaeogeography, Palaeoclimatology, Palaeoecology* 261, 15–29.
- Frijia, G., Parente, M., Iannace, A., 2005. Thermal maturity of the southern apenninic platform unit (southern Italy): constraints from rock-eval pyrolysis Tmax data. *Atti Ticinensi di Scienze della Terra* 10, 95–98.
- Galeotti, S., Rusciadelli, G., Sprovieri, M., Lanci, L., Gaudio, A., Pekar, S., 2009. Sea-level control on facies architecture in the Cenomanian–Coniacian Apulian margin (Western Tethys): a record of glacio-eustatic fluctuations during the Cretaceous greenhouse? *Palaeogeography, Palaeoclimatology, Palaeoecology* 276, 196–205.
- Golubic, S., Radoičić, R., Seong-joo, L., 2006. *Decastronema kotoiri* gen. nov., comb. nov.: a mat-forming cyanobacterium on Cretaceous carbonate platforms and its modern counterparts. *Carnets de Géologie* CG2006, A02.
- van Gorsel, J.T., 1978. Late Cretaceous Orbitoidal foraminifera. In: Hedley, R.G., Adams, C.G. (Eds.), *Foraminifera*, 3. Academic Press, London, UK, pp. 1–120.
- Gradstein, F.M., Ogg, J.G., Smith, A.G., 2004. *A Geologic Time Scale 2004*. Cambridge University Press, Cambridge, UK, 589 p.
- Grötsch, J., Billing, I., Vahrenkamp, V., 1998. Carbon-isotope stratigraphy in shallow-water carbonates: implication for Cretaceous black-shale deposition. *Sedimentology* 45, 623–634.
- Haq, B.U., 2014. Cretaceous eustasy revisited. *Global and Planetary Change* 113, 44–58.
- Hardenbol, J., Thierry, J., Farley, M.B., Jacquin, T., de Graciansky, P.-C., Vail, P.T., 1998. Cretaceous biostratigraphy. In: de Graciansky, P.-C., Hardenbol, J., Jacquin, T., Vail, P.T. (Eds.), *Mesozoic and Cenozoic Sequence Stratigraphy of European Basins*. SEPM, Special Publications, 60, Chart 5.
- Huck, S., Heimhofer, U., Rameil, N., Bodin, S., Immenhauser, A., 2011. Strontium and carbon-isotope chronostratigraphy of Barremian–Aptian shallow-water carbonates: Northern Tethyan platform drowning predates OAE 1a. *Earth Planetary Science Letters* 304, 547–558.
- Huck, S., Heimhofer, U., Immenhauser, A., Weissert, H., 2013. Carbon-isotope stratigraphy of Early Cretaceous (Urgonian) shallow-water deposits: diachronous changes in carbonate-platform production in the north-western Tethys. *Sedimentary Geology* 290, 157–174.
- Huck, S., Rameil, N., Korbar, T., Heimhofer, U., Wiczeorek, T.D., Immenhauser, A., 2010. Latitudinally different responses of Tethyan shallow-water carbonate systems to the Early Aptian oceanic anoxic event (OAE 1a). *Sedimentology* 57, 1585–1614.
- Husinec, A., Harman, C.A., Regan, S.P., Mosher, D.A., Sweeney, R.J., Read, J.F., 2012. Sequence development influenced by intermittent cooling events in the Cretaceous Aptian greenhouse, Adriatic platform, Croatia. *AAPG Bulletin* 96, 2215–2244.
- Immenhauser, A., Hillgartner, H., Van Bentum, E., 2005. Microbial–foraminiferal episodes in the Early Aptian of the southern Tethyan margin: ecological significance and possible relation to oceanic anoxic event 1a. *Sedimentology* 52, 77–99.
- Immenhauser, A., Holmden, C., Patterson, W.P., 2008. Interpreting the Carbon-Isotope Record of Ancient Shallow Epicritic Seas: Lessons from the Recent. In: Pratt, B.R., Holmden, C. (Eds.), *Dynamics of Epicritic Seas*, Geological Association of Canada Special Publication, 48, pp. 135–174.
- Jarvis, I., Mabrouk, A., Moody, R.T.J., De Cabrera, S.C., 2002. Late Cretaceous (Campanian) carbon isotope events, sea-level change and correlation of the Tethyan and Boreal realms. *Palaeogeography, Palaeoclimatology, Palaeoecology* 188, 215–248.
- Jarvis, I., Gale, A.S., Jenkyns, H.C., Pearce, M.A., 2006. Secular variation in Late Cretaceous carbon isotopes and sea-level change: evidence from a new $\delta^{13}\text{C}$ carbonate reference curve for the Cenomanian–Campanian (99.6–70.6 Ma). *Geological Magazine* 143, 561–608.
- Jenkyns, H.C., 1995. Carbon-isotope stratigraphy and paleoceanographic significance of the Lower Cretaceous shallow-water carbonates of Resolution Guyot, mid-Pacific Mountains. In: Winterer, E.L., Sager, W.W., Firth, J.V., Sinton, J.M. (Eds.), *Proceeding of the Ocean Drilling Program, Scientific Results 143*. Ocean Drilling Program, College Station, TX, pp. 99–104.
- Kiessling, W., Flügel, E., Golonka, J., 2003. Patterns of Phanerozoic carbonate platform sedimentation. *Lethaia* 36, 195–226.
- Korbar, T., Glumac, B., Cvetko Tesovic, B., Cadieux, S.B., 2012. Response of a carbonate platform to the Cenomanian–Turonian drowning and OAE2: a case study from the Adriatic Platform (Dalmatia, Croatia). *Journal Sedimentary Research* 82, 163–176.
- Lirer, F., Persico, D., Vigorito, M., 2005. Calcareous plankton biostratigraphy and age of the Middle Miocene deposits of Longano Formation (eastern Matese Mountains, southern Apennines). *Rivista Italiana di Paleontologia e Stratigrafia* 111, 91–108.
- Lohmann, K.C., 1988. Geochemical patterns of meteoric diagenetic systems and their application to studies of paleokarst. In: James, N.P., Choquette, P.W. (Eds.), *Paleokarst*. Springer, Berlin, pp. 58–80.
- Luperto-Sinni, E., Ricchetti, G., 1978. Studio micropaleontologico-stratigrafico di una successione carbonatica del Cretaceo superiore rilevata nel sottosuolo delle Murge sud-orientali. *Rivista Italiana di Paleontologia* 84, 561–666.
- MacLeod, K.G., Huber, B.T., Jiménez-Bercoffo, A., Wendler, I., 2013. A stable and hot Turonian without glacial $\delta^{18}\text{O}$ excursions is indicated by exquisitely preserved Tanzanian foraminifera. *Geology* 41, 1083–1086.
- Maritan, L., Mazzoli, C., Melis, E., 2003. A multidisciplinary approach to the characterization of roman gravestones from Aquileia (Udine, Italy). *Archaeometry* 45, 363–374.
- Marshall, J.D., 1992. Climatic and oceanographic isotopic signals from the carbonate rock record and their preservation. *Geological Magazine* 129, 143–160.
- Masse, J.-P., Steuber, T., 2007. Strontium isotope stratigraphy of Lower Cretaceous rudist bivalves. In: Scott, R.W. (Ed.), *Cretaceous Rudists and Carbonate Platforms: Environmental Feedback*. SEPM, Special Publication, 87, pp. 159–165.
- McArthur, J.M., Howarth, R.J., 2004. Strontium isotope stratigraphy. In: Gradstein, F., Ogg, J., Smith, A. (Eds.), *A Geological Time Scale*. Cambridge University Press, Cambridge, U.K, pp. 96–105.
- McArthur, J.M., Howarth, R.J., Bailey, T.R., 2001. Strontium isotope stratigraphy: lowest version 3. Best-fit to the marine Sr-isotope curve for 0 to 509 Ma and accompanying look-up table for deriving numerical age. *Journal of Geology* 109, 155–170.
- McArthur, J.M., Mutterlose, J., Price, G.D., Rawson, P.F., Ruffell, A., Thirlwall, M., 2004. Belemnites of Valanginian, Hauterivian and Barremian age: Sr-isotope

- stratigraphy, composition ($^{87}\text{Sr}/^{86}\text{Sr}$, $\delta^{13}\text{C}$, $\delta^{18}\text{O}$, Na, Sr, Mg), and palaeo-oceanography. *Palaeogeography, Palaeoclimatology, Palaeoecology* 202, 253–272.
- McArthur, J.M., Thirlwall, M.F., Chen, M., Gale, A.S., Kennedy, W.J., 1993. Strontium isotope stratigraphy in the Late Cretaceous: numerical calibration of the Sr isotope curve and intercontinental correlation for the Campanian. *Paleoceanography* 8, 859–873.
- McArthur, J.M., Kennedy, W.J., Chen, M., Thirlwall, M.F., Gale, A.S., 1994. Strontium isotope stratigraphy for the Late Cretaceous: direct numerical calibration of the Sr-isotope curve for the U.S. Western Interior Seaway. *Palaeogeography, Palaeoclimatology, Palaeoecology* 108, 95–119.
- McArthur, J.M., Rio, D., Massari, F., Castratorì, D., Bailey, T.R., Thirlwall, M., Houghton, S., 2006. A revised Pliocene record for marine $^{87}\text{Sr}/^{86}\text{Sr}$ used to date an interglacial event recorded in the Cockburn Island Formation, Antarctic Peninsula. *Palaeogeography, Palaeoclimatology, Palaeoecology* 242, 126–136.
- McArthur, J.M., Howarth, R.J., Shields, G.A., 2012. Strontium isotope stratigraphy. In: Gradstein, F.M., Ogg, J.G., Schmitz, M., Ogg, G. (Eds.), *The Geologic Time Scale 2012*. Elsevier Science Limited.
- McArthur, J.M., 1994. Recent trends in strontium isotope stratigraphy. *Terra Nova* 6, 331–358.
- Menardi Noguera, A., Rea, G., 2000. Deep structure of the Campanian–Lucanian Arc (Southern Apennine, Italy). *Tectonophysics* 324, 239–265.
- Millán, M.L., Weissert, H., Fernández-Mendiola, P.A., García-Mondejón, J., 2009. Impact of Early Aptian carbon cycle perturbations on evolution of a marine shelf system in the Basque-Cantabrian Basin (Aralar, N Spain). *Earth Planetary Science Letters* 287, 392–401.
- Millán, M.L., Weissert, H., Owen, H., Fernández-Mendiola, P.A., García-Mondejón, J., 2011. The Madotz Urgonian platform (Aralar, northern Spain): paleoecological changes in response to Early Aptian global environmental events. *Palaeogeography, Palaeoclimatology, Palaeoecology* 312, 167–180.
- Miller, K.G., Sugarman, P.J., Browning, J.V., Kominz, M.A., Olsson, R.K., Feigenson, M.D., Hernández, J.C., 2004. Upper Cretaceous sequences and sea-level history, New Jersey Coastal Plain. *GSA Bulletin* 116, 368–393.
- Mostardini, F., Merlini, S., 1986. Appennino Centro-Meridionale: sezioni geologiche e proposta di modello strutturale. *Memorie della Società Geologica Italiana* 35, 177–202.
- Mutti, M., John, C., Knoerich, A., 2006. Chemostratigraphy in Miocene heterozoan carbonate settings; applications, limitations and perspectives. *Geological Society of London Special Publications* 255, 307–322.
- Najarro, M., Rosales, I., Moreno-Bedmar, J.A., de Gea, G.A., Barrón, E., Company, Miguel, Delanoy, G., 2011. High-resolution chemo- and biostratigraphic records of the Early Aptian oceanic anoxic event in Cantabria (N Spain): Palaeoceanographic and palaeoclimatic implications. *Palaeogeography, Palaeoclimatology, Palaeoecology* 299, 137–158.
- Ogg, J.G., Ogg, G., 2008. Late Cretaceous (65–100 Ma time-slice). https://engineering.purdue.edu/Stratigraphy/charts/Timeslices/3_Late_Cret.pdf. Last accessed on August 2014.
- Papp, D.C., Cociuba, I., Lazăr, D.F., 2013. Carbon and oxygen-isotope stratigraphy of the Early Cretaceous carbonate platform of Pădurea Craiului (Apuseni Mountains, Romania): A chemostratigraphic correlation and paleoenvironmental tool. *Applied Geochemistry* 32, 3–16.
- Parente, M., Frijia, G., Di Lucia, M., 2007. Carbon-isotope stratigraphy of Cenomanian–Turonian platform carbonates from southern Apennines (Italy): a chemostratigraphic approach to the problem of correlation between shallow-water and deep-water successions. *Journal of the Geological Society of London* 164, 609–620.
- Parente, M., Frijia, G., Di Lucia, M., Jenkyins, H.C., Woodfine, R.G., Baroncini, F., 2008. Stepwise extinction of larger foraminifera at the Cenomanian–Turonian boundary: a shallow-water perspective on nutrient fluctuations during Oceanic Anoxic Event 2 (Bonarelli Event). *Geology* 36, 715–718.
- Parente, M., Frijia, G., Di Lucia, M., 2010. Comment on “Sea-level control on facies architecture in the Cenomanian–Coniacian Apulian margin (Western Tethys): A record of glacio-eustatic fluctuations during the Cretaceous greenhouse?” by S. Galeotti, G. Rusciadelli, M. Sprovieri, L. Lanci, A. Gaudio and S. Pekar [Palaeogeography, Palaeoclimatology, Palaeoecology 276 (2009) 196–205]. *Palaeogeography, Palaeoclimatology, Palaeoecology* 293, 255–259.
- Patacca, E., Scandone, P., 2007. Geology of the Southern Apennines. In: Mazzotti, A., Patacca, E., Scandone, P. (Eds.), *CROP-04, Bollettino Società Geologica italiana (Ital.J.Geosci.)*, Special Issue, 7, pp. 75–119.
- Patterson, W.P., Walter, L.M., 1994. Depletion of ^{13}C in seawater ΣCO_2 on modern carbonate platforms: significance for the carbon isotopic record of carbonates. *Geology* 22, 885–888.
- Philip, J., 2003. Peri-Tethyan neritic carbonate areas: distribution through time and driving factors. *Palaeogeography, Palaeoclimatology, Palaeoecology* 196, 19–37.
- Prokoph, A., Shields, G.A., Veizer, J., 2008. Compilation and timeseries analysis of a marine carbonate $\delta^{18}\text{O}$, $\delta^{13}\text{C}$, $^{87}\text{Sr}/^{86}\text{Sr}$ and $\delta^{34}\text{S}$ database through Earth history. *Earth-Science Reviews* 87, 113–133.
- Ruberti, D., Toscano, F., 2002. Microstratigraphy And Taphonomy Of Rudist Shell Concentrations In Upper Cretaceous Limestones, Cilento Area (Southern Italy). *Geobios* 24, 228–240.
- Ruberti, D., Toscano, F., Carannante, G., Simone, L., 2006. Rudist lithosomes related to current pathways in Upper Cretaceous temperate-type, inner shelves: a case study from the Cilento area, southern Italy. In: Pedley, H.M., Carannante, G. (Eds.), *Cool-Water Carbonates: Depositional Systems and Palaeoenvironmental Controls*. Geological Society Special Publications, 255, pp. 179–195.
- Ruberti, D., Carannante, G., Simone, L., Sirna, G., Sirna, M., 2007. Sedimentary processes and biofacies of Late Cretaceous low-energy carbonate ramp systems (southern Italy). In: Scott, R.W. (Ed.), *Cretaceous Rudists and Carbonate Platforms: Environmental Feedback*, SEPM Special Publication, 87, pp. 57–70.
- Sartoni, S., Crescenti, U., 1962. Ricerche biostratigrafiche nel Mesozoico dell'Appennino meridionale. *Giornale di Geologia* 29, 161–293.
- Schettino, A., Turco, E., 2011. Tectonic history of the western Tethys since the Late Triassic. *GSA Bulletin* 123, 89–105.
- Schlager, W., 2000. Sedimentation rates and growth potential of tropical, cool-water and mud-mound carbonate systems. In: Insalaco, E., Skelton, P.W., Palmer, T.J. (Eds.), *Carbonate Platform Systems: components and interactions*. Geological Society Special Publications, 178, pp. 217–227.
- Schlagintweit, F., Husinec, A., Jez, J., 2014. *Siphodinarella costata* n. gen., n. sp., a new benthic foraminifer from the Coniacian of the Adriatic Carbonate Platform (Slovenia, Croatia). *Facies* 60, 133–145.
- Schlagintweit, F., Sander, D., 2008. *Tetraxiella? floriforma* n. sp. and other benthic foraminifera from the Gosau Group of the Northern Calcareous Alps, Austria. *Austrian Journal Earth Sciences* 101, 17–26.
- Schlüter, M., Steuber, T., Parente, M., 2008. Chronostratigraphy of Campanian–Maastrichtian platform carbonates and rudist associations of Salento (Apulia, Italy). *Cretaceous Research* 29, 100–114.
- Scholle, P.A., Arthur, M.A., 1980. Carbon-isotope fluctuations in Cretaceous pelagic limestones: potential stratigraphic and petroleum exploration tool. *AAPG Bulletin* 64, 67–87.
- Schroeder, R., van Buchem, F.S.P., Cherchi, A., Baghbani, D., Vincent, B., Immenhauser, A., Granier, B., 2010. Revised orbitolinid biostratigraphic zonation for the Barremian – Aptian of the eastern Arabian Plate and implications for regional stratigraphic correlations. *GeoArabia Special Publication* 4 (1), 49–96.
- Selli, R., 1957. Sulla trasgressione del Miocene nell'Italia meridionale. *Giornale di Geologia* 2, 1–54.
- Selli, R., 1962. Il Paleogene nel quadro della Geologia dell'Italia Centro-Meridionale. *Memorie della Società Geologica Italiana* 3, 737–789.
- Servizio Geologico d'Italia, 2010. Carta Geologica d'Italia 1:50000. Sala Consilina, Foglio 504.
- Sgrosso, L., 1988. Nuovi elementi per un più articolato modello paleogeografico nell'Appennino meridionale. *Memorie della Società Geologica Italiana* 41, 203–219.
- Simone, L., Carannante, G., Ruberti, D., Sirna, M., Sirna, G., Laviano, A., Tropeano, M., 2003. Development of rudist lithosomes in the Coniacian–Lower Campanian carbonate shelves of central–southern Italy: high-energy vs low-energy settings. *Palaeogeography, Palaeoclimatology, Palaeoecology* 200, 5–29.
- Skelton, P.W., 2003. Changing Climate and biota – the marine record. In: Skelton, P.W. (Ed.), *The Cretaceous World*. Cambridge University Press, Cambridge, pp. 163–184.
- Stampfli, G.M., Mosar, J., 1999. The making and becoming of Apulia. *Memorie Scienze Geologiche* 51, 141–154.
- Stein, M., Arnaud-Vanneau, A., Adatte, T., Fleitmann, D., Spangenberg, J., Föllmi, K.B., 2012. Paleoenvironmental and paleoecological change on the northern Tethyan carbonate platform during the late Barremian –earliest Aptian. *Sedimentology* 59, 939–963.
- Steuber, T., 1999. Isotopic and chemical intra-shell variations in low-Mg calcite of rudist bivalves (Mollusca: Hippuritacea) e disequilibrium fractionations and Late Cretaceous seasonality. *International Journal Earth Sciences* 88, 551–570.
- Steuber, T., 2001. Strontium isotope stratigraphy of Turonian–Campanian Gosau-type rudist formations in the Northern Calcareous and Central Alps (Austria and Germany). *Cretaceous Research* 22, 429–441.
- Steuber, T., 2003. Strontium isotope chemostratigraphy of rudist bivalves and Cretaceous carbonate platforms. In: Gili, E., Negra, M.E.H., Skelton, P.W. (Eds.), *North African Cretaceous Carbonate Platform Systems*, NATO Science Series, IV, Earth and Environmental Sciences, 28, pp. 229–238.
- Steuber, T., Schlüter, M., 2012. Strontium-isotope stratigraphy of Upper Cretaceous rudist bivalves: biozones, evolutionary patterns and sea-level change calibrated to numerical ages. *Earth-Science Reviews* 114, 42–60.
- Steuber, T., Korbart, T., Jelaska, V., Gusic, I., 2005. Strontium isotope stratigraphy of Upper Cretaceous platform carbonates of the island of Brač (Adriatic Sea, Croatia): implications for global correlation of platform evolution and biostratigraphy. *Cretaceous Research* 26, 741–756.
- Steuber, T., Mitchell, S.F., buhl, D., Gunter, G., Kasper, H.U., 2002. Catastrophic extinction of Caribbean rudist bivalves at the Cretaceous-Tertiary boundary. *Geology* 30, 999–1002.
- Steuber, T., Parente, M., Hagmaier, M., Immenhauser, A., van der Kooij, B., Frijia, G., 2007. Latest Maastrichtian species-rich rudist associations of the Apulian Margin of Salento (S Italy) and the Ionian Islands (Greece). In: Scott, R.W. (Ed.), *Cretaceous Rudists and Carbonate Platforms: Environmental Feedback*. SEPM, Special publication, 87, pp. 151–157.
- Stoll, H.M., Schrag, D.P., 2000. High resolution stable isotope records from the Upper Cretaceous rocks of Italy and Spain: glacial episodes in a greenhouse planet? *GSA Bulletin* 112, 308–319.
- Strohmer, C.J., Steuber, T., Ghani, A., Barwick, D.G., Al-Mazrooei, S.H.A., Al-Zaabi, N.O., 2010. Sedimentology and chemostratigraphy of the Hawar and Shuaiba depositional sequences, Abu Dhabi, United Arab Emirates. *GeoArabia Special Publication* 4 (2), 341–365.
- Swart, P.K., 2011. Is there really a mixing-zone stable carbon and oxygen isotope signal? Abstracts book, 28th IAS Meeting of Sedimentology 2011, Zaragoza, Spain.
- Tesovic, B.C., Glumac, B., Buckovic, D., 2011. Integrated biostratigraphy and carbon isotope stratigraphy of the Lower Cretaceous (Barremian to Albian) Adriatic-

- Dinaridic carbonate platform deposits in Istria, Croatia. *Cretaceous Research* 32, 301–324.
- Vahrenkamp, V., 1996. Carbon isotope stratigraphy of the Upper Kharab and Shuaiba Formations: implications for the Early Cretaceous evolution of the Arabian Gulf Region. *AAPG Bulletin* 80, 647–662.
- Vahrenkamp, V.C., 2010. Chemostratigraphy of the Lower Cretaceous Shu'aiba Formation: A $\delta^{13}\text{C}$ reference profile for the Aptian Stage from the southern Neo-Tethys Ocean. *GeoArabia Special Publication* 4-1, 107–137.
- Velic, I., 2007. Stratigraphy and palaeobiogeography of Mesozoic benthic foraminifera of the Karst Dinarides (SE Europa). *Geologia Croatica* 60, 1–113.
- Venturini, S., 2005. *Lévento a Keramosphaerina tergestina*: considerazioni bio-cronostratigrafiche. *Natura Nascosta* 31, 15–22.
- Vicedo, V., Frijia, G., Parente, M., Caus, E., 2011. The late Cretaceous genera *Cuvillierinella*, *Cyclopseudomia* and *Rhapydionina* (Rhapydioninidae, Foraminifera) in shallow water carbonates of Pylos (Peloponnese, Greece). *Journal of Foraminiferal Research* 41, 41–52.
- Vicedo, V., Caus, E., Frijia, G., 2013. Late Cretaceous alveolinaceans (Larger foraminifera) of the Caribbean palaeobioprovince and their stratigraphic distribution. *Journal of Systematic Palaeontology* 11, 1–25.
- Wagner, P.D., 1990. Geochemical stratigraphy and porosity controls in Cretaceous carbonates near the Oman Mountains. In: Robertson, A.H.F., Searle, M.P., Ries, A.C. (Eds.), *The Geology and Tectonics of the Oman Region*. Geological Society Special Publication, 49, pp. 127–137.
- Weber, J.N., Woodhead, P.M.J., 1969. Factors affecting the carbon and oxygen isotopic composition of marine carbonate sediments-II. Heron Island, Great Barrier Reef, Australia. *Geochimica Cosmochimica Acta* 33, 19–38.
- Weissert, H., Joachimski, M., Sarnthein, M., 2008. Chemostratigraphy. *Newsletters in Stratigraphy* 42, 145–179.
- Wendler, I., 2013. A critical evaluation of carbon isotope stratigraphy and biostratigraphic implications for Late Cretaceous global correlation. *Earth-Science Reviews* 126, 116–146.
- Wissler, L., Funk, H., Weissert, H., 2003. Response of Early Cretaceous carbonate platforms to changes in atmospheric carbon dioxide levels. *Palaeogeography, Palaeoclimatology, Palaeoecology* 200, 187–205.
- Wissler, L., Weissert, H., Buonocunto, F.P., Ferreri, V., D'Argenio, B., 2004. Calibration of the Early Cretaceous time scale: a combined chemostratigraphic and

cyclostratigraphic approach to the Barremian-Aptian interval Campania Apennines and southern Alps (Italy). In: D'Argenio, B., Fischer, A.G., Premoli Silva, I., Weissert, H., Ferreri, V. (Eds.), *Cyclostratigraphy, approaches and case histories*. SEPM Special Publication, 81, pp. 123–134.

Appendix

List of taxa mentioned in the text.

- Accordiella conica* Farinacci, 1962
Biconcava bentori Hamaoui and Saint-marc, 1970
Calveziconus lecalvezae Caus and Cornella, 1981
Chrysalidina gradata D'Orbigny, 1839
Cisalveolina fraasi (Gümbel, 1872)
Coxites zubairensis Smout, 1956
Dicyclina schlumbergeri Munier-Chalmas, 1887
Keramosphaerina tergestina (Stache, 1889)
Moncharmontia apenninica (De Castro, 1966)
Murgella lata Luperto Sinni, 1966
Nezzazinella cf. aegyptiaca Said and Kenaway, 1957
Nummoloculina cf. Irregularis Decrouez and Radoičić, 1977
Pseudocyclammina sphaeroidea Gendrot, 1968
Pseudolituonella reicheli Marie, 1954
Pseudorhapydionina dubia (De Castro, 1965)
Pseudorhipidionina casertana (De Castro, 1965)
Reticulinella fleuryi Cvetko, Gusic and Schroeder, 1997
Reticulinella kaeveri Cherchi, Radoičić and Schroeder, 1989
Rotorbinella scarsellai Torre, 1966
Scandonea mediterranea De Castro, 1974
Scandonea samnitica De Castro, 1971
Siphodinarella costata Schlagintweit, Husinec and Jez, 2014
Trochospira avnimelechi Hamaoui and Saint Marc, 1970
Vidalina radoicicae Cherchi and Schroeder, 1986